RATIONAL DESIGN OF DEEP EUTECTIC SOLVENTS FOR ABSORPTION OF H_2S FROM NATURAL GAS

Mirat Karibayev, Bachelor in Chemistry

Submitted in fulfillment of the requirements for the degree of Masters of Science in Chemical and Materials Engineering

School of Engineering and Digital Sciences
Department of Chemical and Materials Engineering
Nazarbayev University

53 Kabanbay Batyr Avenue,
Nur-Sultan, Kazakhstan, 010000

Supervisors: Shah, Dhawal & Torkmahalleh, Mehdi Amouei

April 2020

Abstract

Novel Deep Eutectic Solvents (DESs) are being developed, which are non-flammable and biodegradable. These DESs are used in application for organic synthesis, metal processing, gas absorption, and removal of different undesired impurities in oil & gas industries. For instance, a combination of caprolactam (CPL) and tetrabutylammonium halides (1:1, mole ratio), as the DES, has indicated the highest efficiency for desulfurization of natural gas. We herein implement ab-initio and molecular dynamic simulations to explore the formation of CPL based type III DESs. The simulations show ~15% decline in the ionic interactions of tetrabutylammonium halides and ~92% decline in the hydrogen bonds between CPL, thereby explaining the rapid decline in the melting point as noted in experiments during the formation of DES. Moreover, ab-initio and molecular dynamic (MD) simulations of the caprolactam based DES with hydrogen sulfides and methane's were conducted in order to mimic the industrial natural gas sweetening process. Efficient absorption of hydrogen sulfide from natural gas at various process parameters (5000/10000 ppm H_2S, at 25/ 60 ^oC, and at 1/10 bar) can be highlighted from the molecular dynamic simulations. The results revealed strong intermolecular interactions between the anions of the caprolactam based DESs and hydrogen sulfide (H_2S), with interaction energies ~10 folds higher than methane (CH_4)/hydrogen sulfide (H_2S), explaining the mechanism of desulfurization by these DESs. The ab-initio and molecular dynamics simulations were computed via the implementation of GAUSSIAN16, GROMACS software's. The given work also illustrates that two DESs, namely a combination of choline chloride (ChCl) with urea, and monoethanolamine (MEA) with methyltriphenylphosphonium bromide (MTPPBr) were implemented to compare their capacity to absorb hydrogen sulfide (H_2S), however we observed that the CPL based DESs are highly efficient, particularly at low fuel:DES mole ratios, low temperatures, and at low pressures.

Acknowledgments

Initially, I would like to thank my supervisor Dr. Dhawal Shah and Mehdi Torkmahalleh for their valuable advices and constant supports. I am proud of being under their supervision during this master thesis period. Moreover, I want to express my great thanks the Nazarbayev University, especially School of Engineering and Digital Sciences for golden education and computational support by machines to perform ab-initio calculations and molecular dynamic simulations.

Table of Contents

List of Abbreviations

ATB – Automated Topology Builder

LINCS – Linear Constraint (solver, algorithm)

LJ - *Lennard-Jones (potential)*

MD – Molecular Dynamics

MEA – Monoethanolamine

MTPPBr -Methyl triphenyl phosphonium bromide

ChCl - choline chloride

CPL – caprolactam

TBABr -tetrabutylammonium bromide

TBACl - tertbutylammonium chloride

DES - Deep Eutectic Solvents

DFT – Density Functional Theory

NVT – a MD simulation, where number of molecules, volume, and temperature are held constant

NPT – a MD simulation, where number of molecules, pressure and temperature are held constant

RDF – Radial Distribution Function

s (ps, ns) – Second (picosecond, nanosecond)

VMD – Visual Molecular Dynamics

List of Figures

List of Tables

Chapter 1 – Introduction

1.1 Background

There are plenty of natural gas reserves available on the earth. Considering these, the global consumption of natural gas is predicted to exceed petroleum and coal in the future. Natural gas play critically important role in daily life as a clean energy source, especially in Kazakhstan. Therefore, in Kazakhstan, natural gas consumption has been increasing per capita from 0.444 ft^3/day to 1.880 ft^3/day from 2004 to 2018 [1]. The chemical composition of natural gas is primarily methane (CH_4), but it also includes other components such as ethane (C_2H_6), propane (C_3H_8), normal butane (C_4H_{10}), pentanes (C_5H_{12}), carbon dioxide (CO_2), hydrogen sulfide (H_2S), nitrogen (N_2), and helium (He) [1]–[3]. While the H_2S is in small amount (usually <1 % in volume), it needs to be removed due to environmental concerns and government regulations. H_2S is a toxic and a corrosive gas which also creates various issues during the natural gas processing including corrosion of pipelines & tanks. Moreover, regulations of several governments and organizations demand the allowable limit of H_2S in natural gas be reduced to 10 ppm [4], [5].

In over 95 % of all gas processing plants in the US, hydrogen sulfide is removed from natural gas by chemical absorption. Typical solvents that are generally used for chemical absorption are based on alkanolamine including monoethanolamine, diglycolamine, diethanolamine, diisopropanolamine, methyldiethanolamine and others [1]. These amine solvents have high volatility, are economically expensive as it consumes high energy for regeneration, leads to formation of unwanted by products and limited capture capacity during natural gas plant processing [4], [6], [7]. In this regard, various ionic liquids (ILs) have been expected as an alternative solvent for desulfurization of natural gas. Unfortunately, Ionic Liquids have not been applied in industry because of their poor biocompatibity, sustainability and high cost [4], [8], [9]. Meanwhile, more recent attention has been on progress of several new Deep Eutectic Solvents

(DESs) for natural gas upgrading. DESs are considered as Ionic Liquid analogues. Deep Eutectic Solvents are a eutectic mixture of Lewis or Brønsted acids and bases that have several cationic and anionic species [3]. Moreover. DESs are non-flammable, biodegradable, environmentally benign, and are ease to manufacture in terms of cost and processes involved [4]. There are various applications of DESs such as gas adsorption, metal processing, organic synthesis, and removal of various unwanted impurities in oil & gas industry and others [5].

1.2 Objective

More recently, DESs have been developed for absorption of H_2S from natural gas. While experiments show effectiveness of these DESs, the mechanism of absorption and their functioning remains obscured. A key to our proposed work was simulation of the DES with CH_4 and H_2S that were explored to understand the natural gas upgrading process, as existing research works cover only experimental studies on absorption of pure H_2S. Hence, our objective herein is to explore these new DESs and our main goals are (i) determine the molecular interactions leading to the formation of the caprolactam based DESs, (ii) determine the mechanism of absorption of H_2S by these DESs, and (iii) analyze the effect of process parameters (temperature, pressure, and concentration) on natural gas sweetening process.

Combination of tetrabutylammonium halides with caprolactam at a ratio of 1:1 was considered as DES, while CH_4 with H_2S was applied to model natural gas. The simulations were performed with use of GAUSSIAN16, GROMACS tools. The following work also studies that the applications of other DESs, namely a combination of choline chloride with urea, and monoethanolamine with methyltriphenyl phosphonium bromide in natural gas sweetening process. Furthermore, effect of different desulfurization process parameters including concentration, temperature, and pressure were studied in order to understand their effect on the removal efficiency.

Chapter 2 - Literature Review

2.1 Natural Gas Sweetening

The natural gas upgrading is a removal of H_2S and CO_2 from gases in petrochemical plants, natural gas and other industries. H_2S and CO_2 can be removed selectively or simultaneously during the gas sweetening processes by depending on the quality and quantity of acid gases present in natural gas [3].

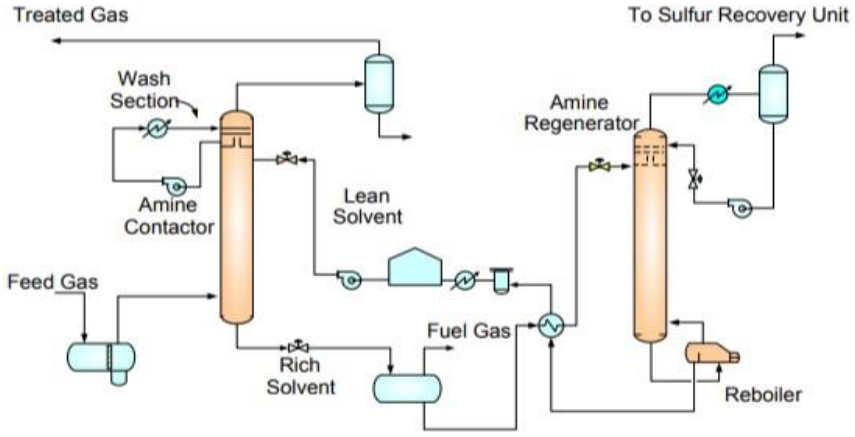

Figure 2.1: Process flow diagram for natural gas sweetening [1]

The process flow diagram for natural gas upgrading varies little through different implemented aqueous amine solvents. However, the general process flow scheme for amine solvents is illustrated on Figure 2.1. The feed natural gas is scrubbed in an amine solvent contractor that consists of an absorber section and a water wash section. The absorber section removes H_2S from the feed natural gas through chemical absorption of lean amine based solvent which leads to generation of treated gas and rich solvent. The water wash section recovers amine solvents from the treated gas and rich solvent. The water wash section recovers amine solvents from the treated gas to decrease amine make up requirements and reduce fouling in the molecular sieve unit [1]. Following that, rich amine is flashed in amine flash drum to remove dissolved gases. Then, the rich solution of amine form the flash drum passes by the amine heat exchanger to preheat rich solvent to the regenerator. The rich amine regenerated as lean amine through stripping of acid gases in presence of stream or other heating medium. Finally, the lean amine is pumped, cooled,

and recycled back to the amine absorption column [1].

Amine solvents are classified into three groups including primary amines (monoethanolamine, diglycolamine), secondary amine (diisopropanolamine, diethanolamine) and tertiary amine (methyl diethanolamine, triethanolamine) [1], [10]. Primary amines are stronger bases in comparison with secondary amines and can chemically react with H_2S and CO_2 [10], [11]. In addition, different mixtures of amine solvents were studied to remove unwanted impurities from natural gas. For instance, Jou and his research team studied a mixture of tetramethylene sulfone with diisopropanol in the presence of water [12]. The authors also replaced the diisopropanolamine with methyldiethanolamine [10], [12].

The common problems in implementation of amine solvents are degradation and foaming during the acid gases removal process. The degradation of amine based solvents can be caused by carbon disulfide (CS_2), oxygen (O_2), carbonyl sulfide (COS), carbon dioxide (CO_2), and other chemicals which lead to corrosion of the equipment [1], [10], [12]. Meanwhile, foaming of amine solvents could be explained by suspended solids, liquid hydrocarbons, and condensation of lean solvent, amine decomposition and by-product degradation and others. In addition, the vaporization, chemical losses and mechanical losses leads to amine solvent losses [1].

2.2 Deep Eutectic Solvents (DESs)

Deep Eutectic Solvents (DESs), alternatively, are recently proposed as novel solvents with potential applications in desulfurization [13], [14]. DESs are widely known as analogues of ILs because of similarities in their properties. However, despite their similarities in physical properties, they are, in fact, two different types of solvents. DESs are a eutectic mixture of Lewis or Brønsted acids and bases that have several cationic and anionic species, while ILs are basically solvents that are produced primarily of one discrete type of cation and anion [4], [6], [15]. Moreover, many DESs are biodegradable, non-flammable, have low vapor pressure, and also low cost, which makes them very promising, and additional advantage over ILs, in large scale applications [16]. The key property of DESs is low melting point, since DES itself is being formed at a eutectic composition, as shown in Figure 2.2. [17]

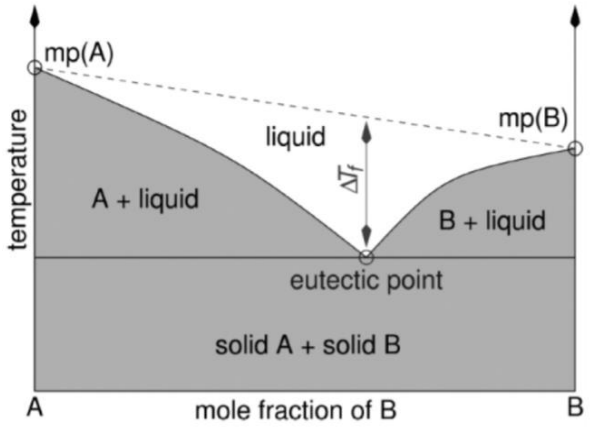

Figure 2.2: Formation of eutectic point in a phase diagram [18]

The Figure 2.2 illustrates a significant decrease in the melting point of the mixture, in comparison with melting points of either of the components. Thus, even though DES is being formed from solid components with very high melting points, mixture can be liquid at room temperature. DESs generally classified into 4 main categories depending on different combinations and types of components.

Table 2.1: Classification of Deep Eutectic solvents [17]

type	general formula	terms
I	$Cat^+X^-zMCl_x$	M = Zn, Sn, Fe, Al, Ga, In
II	$Cat^+X^-zMCl_x{\cdot}yH_2O$	M= Cr, Co, Cu, Ni, Fe
III	Cat^+X^-zRZ	Z= $CONH_2$, COOH, OH
IV	$MCl_x + RZ = MCl_{x-1}^+ \cdot RZ + MCl_{x+1}^-$	M = Al, Zn and Z = $CONH_2$, OH

Type I DESs are mixtures of quaternary ammonium salts and metal chlorides; Type II are mixtures of quaternary ammonium salts and metal chloride hydrates; Type III are mixtures of quaternary ammonium salts and hydrogen bond donors; and lastly Type IV are mixtures of metal chloride hydrates and hydrogen bond donors (Table 2.1) [18]. Similar to ILs, the components of DESs can be tailored as desired for the application. The first report of DES came in 2004, wherein Abbott et al. report a mixture of choline chloride and urea at 1:2 molar ratio, and the resultant mixture showed depression in melting point of more than 200 ^{0}C [17]. Since then many DESs have been reported, with a combination of salt and hydrogen bond donor (HBD). In addition, type I, II and IV DESs contain metal salts which are toxic, while only type III eutectics have low inherited toxicity.

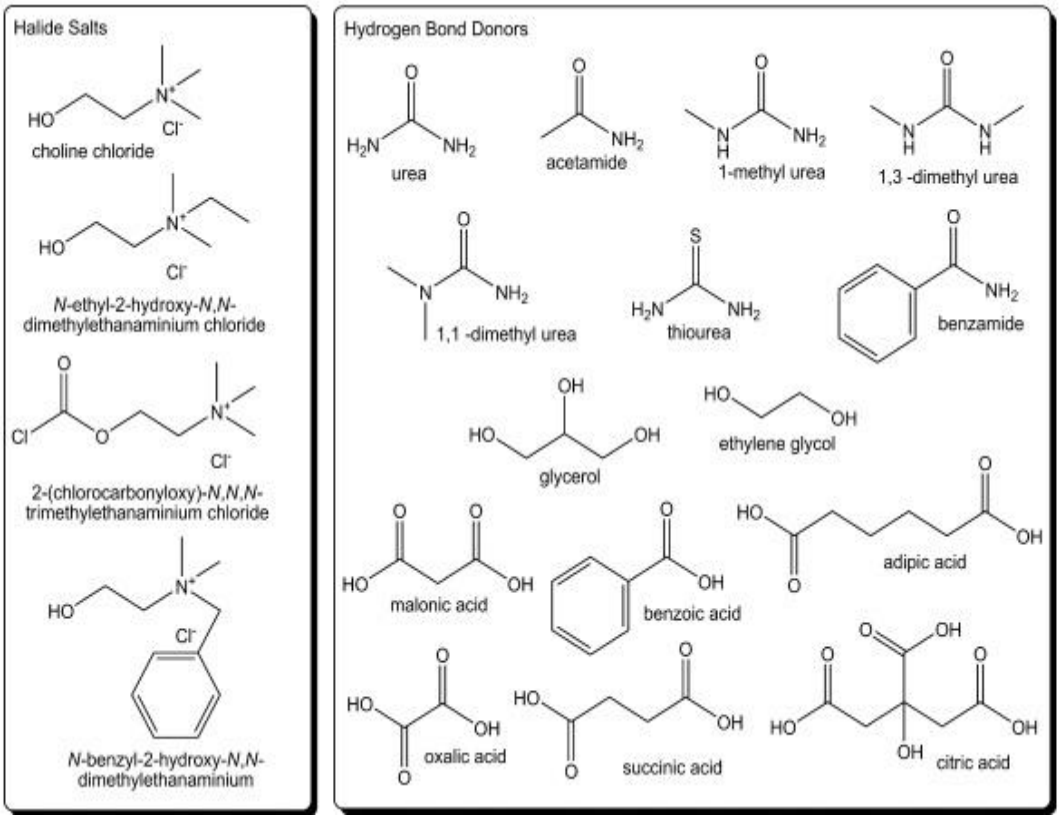

Figure 2.3: HBDs and salts used in the literature for production of DESs [18]

Gracia et al. (2015) have compiled a comprehensive list of such salts and HBDs (Figure 2.3) [18]. Some of the commonly used salts are choline chloride, choline nitrate, ethylammonium chloride, tetrabutylammonium chloride, tetrabutylammonium bromide, benzyltriphenylphosphonium chloride, methyltriphenylphosphonium bromide, 1-butyl-3-methylimidazolium chloride, etc., and the commonly used HBDs are urea, ethylene glycol, glycerol, PEGs, glucose, xylitol, malonic acid, arginine, lactic acid, phenol, monoethanolamine, $FeCl_3$, $ZnCl_2$, etc. While the lists are broad and too many combinations are possible, DES based on choline chloride are used more often than others.

2.3 Formation of DESs

Abbot with his research group suggested a *hole theory* to understand the intmolecular formation mechanism of DES. The *hole theory* explains movement of ions within DES and measures various physical properties including viscosity, surface tension, density, and conductivity. *Hole theory* assumes that vacant places are created during melting process due to

fluctuations that are generated thermally in local density and have constant flux in those holes. Consequently, it is much easier to move into a space for an ion with a smaller size [19]. DES will have a hole-size distribution at any time and an ion will travel to it if there is a hole with an appropriate dimension. It ensures that only some parts of the ions can move and the viscosity of DES can be decreased insignificantly as a consequence. It was noted, however, that the hole sizes were larger with higher temperature, leading to lower viscosities. Generally, knowing the probability of hole formation in the liquid, it is easy to understand DES formation and also design new DESs with low viscosities.

In addition to the hole theory and its implementation in DESs tailoring, it is worth to mentioning the presence of hydrogen bond interactions in DES between hydrogen bond acceptor and hydrogen bond donor [20]. Molar ratio between hydrogen bond donor (HBD) and hydrogen bond acceptor (HBA) plays critical role in determination of eutectic point. From the Table 2.2, it is clearly seen that the difference in melting points depends on the molar ratio of HBD and HBA [20].

Table 2.2: Freezing points for DES at 101.3 kPa [20]

mol %BTEAC	Freezing point (K)		
	DES A	DES B	DES C
30	275	308	301
40	279	301	284
50	289	299	278
60	293	300	306
70	314	330	335

In Table 2.2, DES A is a mixture of p-toluene sulfonic acid (PTSA) and benzyl triethylammonium chloride (BTEAC), DES B is triethylammonium chloride (TEAC) with citric acid (CA), DES C is benzyl triethylammonium chloride (BTEAC) with oxalic acid (OX). As can be seen clearly, the molar ratio of hydrogen bond donor (BTEAC) affects the melting point of the formed DESs. Several research works have been showed to correlate the strong depression in the melting point in DES with the number of hydrogen bonds present in the system. For instance, in

previous works of Shah and Mjalli, they have used molecular dynamics simulations to count in the number of hydrogen bonds in the choline chloride (ChCl) based DESs and their aqueous solutions [21]. Interestingly the mixtures with less number of hydrogen bonds indeed had low melting points. However, not all Deep Eutectic Solvents have hydrogen bonds and in such cases, depression in the freezing point is associated with exchange of ions between compounds and the complex structure formed. For instance, Abbott et al. in their research work studied the formation of choline chloride: zinc chloride DES (ChCl:$ZnCl_2$), where ions pass the following equilibrium exchange reaction [22].

$$ZnCl_2 + ChCl \leftrightarrow Ch^+ + ZnCl_3^-$$

Chloride anion is a strong base and it shifts the reaction to the right resulting in formation of $ZnCl_3^-$. Furthermore, Mjalli and Shah, (CET, 2015), observed similar exchange of ions in tetrabutylphosphonium bromide (TBPBr) and $FeCl_3$ based DES [21].

2.4 Application of DESs

Due to their interesting properties, DESs have seen a wide range of applications in various industries, such as metal processing, gas adsorption, organic synthesis, and in the oil & gas industry. The major advantages of DESs are that they are biodegradable, liquid at the ambient temperature, have low volatility, high conductivity, and have good solubility of metal salts, and are thus reasonable choice for solvents in several processes [23].

2.4.1 Metal processing

One of the current applications of DESs are in metal processing is electroplating, considering their high solubility for metal salts, oxides and hydroxides. DES can avoid the passivation issues which occur because of formation of non-soluble compounds ate the electrodes surface [23]. The use of DES does not require the consumption of hazardous complexing agents, for example, cyanide which is toxic and has high disposal cost. In additionally to that, water, which is currently used, is not necessarily a sustainable solvent, despite the fact that it is non-toxic, since it needs treatment steps before being disposed to the water courses [16]. Another application is

metal electropolishing, wherein Deep Eutectic Solvents are being employed over conventional aqueous acid based solutions, because of the high current efficiency. One of examples of DESs that has been commercially applied for electroplating are choline chloride with ethylene glycol [23].

2.4.2 Synthesis of organic compounds

With its "green" behavior and ability to be selectively towards a particular reaction, DESs have also been employed in several organic synthesis processes. Shankarling with his research team applied a combination of choline chloride and urea mixture as the DES for Perkin reaction, bromination and reduction of epoxides [24]. The detailed mechanism of those reactions illustrated in Figure 2.4.

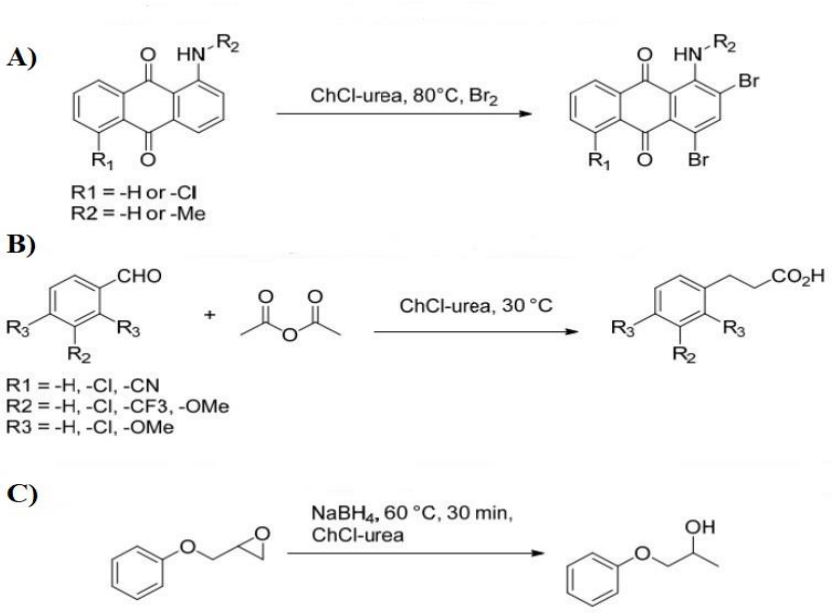

Figure 2.4: A) Bromination, B) Perkin reaction, and C) reduction of epoxides via DES [25]

Commonly, the synthesis of those products requires use of toxic solvents, strong acids, and elevated temperatures and therefore application of DESs could be a good alternative to avoid those issues. Additionally, DESs were used in the N-alkylation of aromatic amines for selectivity purposes [25]. In the other works, Fischer indole annulations was performed with a combination of choline chloride and zinc chloride in 1:2 molar ratio, as the DES in the presence of hot

polyphosphoric acid which is followed by addition of water to complete filtration of desired product. Acid residue disposal can have a negative impact to the environment. Although, implementation of DES could help to avoid this issue and additionally, can give high yield of desirable products[26].

2.4.3 Gas absorption

Every year, fossil fuel consumption rises with growing demand for energy and with this emission of carbon dioxide also increases. In addition, the cheap and abundant sources of energy found naturally in liquid oil and gaseous hydrocarbons have been used by humans for well over a century, with the primary use serving as fuel for transportation needs. The full oxidation of hydrocarbons, however, produces carbon dioxide and water as the ultimate chemical products, in addition to the energy produced.

Each 4 liters of burned gasoline releases to the atmosphere about 10 kilograms of carbon dioxide. Considering these, the rates of the known greenhouse gas carbon dioxide in the atmosphere critically rise [27]. On the other hand, the traditional solvents such as ethanolamine, monoethanolamine, zeolite, activated carbon and polymer adsorbents is the current methods which is implemented for post combustion carbon dioxide capture and storage [27]. In addition, since some traditional solvents could not be easily synthesized because of their toxicity and high process cost, DESs have been proposed as an alternative. For instance, the mixture of activated carbon with choline chloride/glycerol in 1:2 molar ratios illustrated a high carbon dioxide adsorption capacity [28].

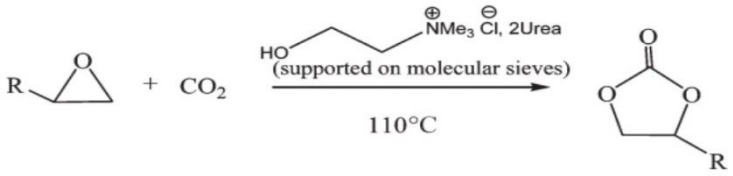

Figure 2.5: Cyclic carbonate synthesis from epoxides with CO_2 in the DES [28]

Zhu et al. reported another interesting work in which the synthesis of cyclic carbonates from epoxides in the presence of carbon dioxide was successfully performed via using choline chloride/urea (DES) as a catalyst (Figure 2.5) [29]. In addition, a combination of

tetramethylammonium chloride and lactic acid at molar ratio 1:2, as the environmentally benign and biodegradable DES has shown the high adsorption capacity for post combustion carbon dioxide capture and storage [30].

2.4.4 Oil and gas industry

The presence of organic sulfides in the fuel is one of the reasons for this ecological issue. Burning the fuel a with high sulfur content results in the release of toxic gaseous sulfur oxides (SOx) into the atmosphere, resulting in acid rain, catalysts degradation, and corrosion of constructions [31]. Considering these, the concentration of aromatic sulfur compounds in fuels is always under constant control by government. Currently, the solvents such as sulfone, ethylene glycol are implemented in the desulfurization process of fuel. DESs are becoming cheap, environmentally benign and effective solvents to remove organic sulfur containing compounds from fuels.

One of the earliest researches was performed in 2013 on desulfurization of fuel through DESs [31]. Namely, all of the DES samples contained coordinated metal ions, which improved the efficiency of extracting organic sulfur compounds from fuels. Experimentally, the researchers concluded that the efficiency of the desulfurization process depends on various factors such as concentration of organic sulfur compounds, composition of DES to fuel, operating temperature and pressure. It was observed that increasing the DES mass ratio to the fuel improves the desulfurization efficiency and demonstrated successful recyclability [32]. In general, it was proposed that the mechanism of the desulfurization through DES is depending on hydrogen bonding interactions and coordination of metal ions [32]. In addition, DES could be implemented for extraction of glycerol from biodiesel which is environmentally friendly biofuel made from animal fats or vegetable oils. The chemical composition of biofuel is long chain alkyl esters which are obtained by transesterification. The glycerol is an unwanted by-product of this process and it raises the viscosity which can cause damages in the injection parts of diesel engines. Nowadays, water is implemented to remove the glycerol from the fuel; however, it leads to loss of product and additionally, this water requires treatment procedures before disposing into waste. Consequently, a combination of ammonium salt and glycerol at molar ratio 1:2, as the DES has

shown 99% efficiency for extraction of glycerol from the fuel [33]. Finally, DESs have been also implemented in absorption of acid gases such as CO_2 and H_2S from natural gas. The Chapter I discussed the current desulfurization methods and this chapter will now focus more on the removal of H_2S from natural gas using several new DES.

Since 2010, several research papers have been written on the use of DESs in desulfurization of natural gas. Most of these research articles concentrate on the implementation of chemical absorption method for deep desulfurization of natural gas and depending on the Deep Eutectic Solvents chosen; the solubility H_2S in natural gas can reach 1.58 mol H_2S/kg DES. Some DESs have been experimentally shown efficient in absorbing H_2S. Guo et al., for example, showed that a DES made from carpolactam and tetrabutylammonium halides can readily absorb and desorb H_2S as can be seen from the Figure 2.6 [34].

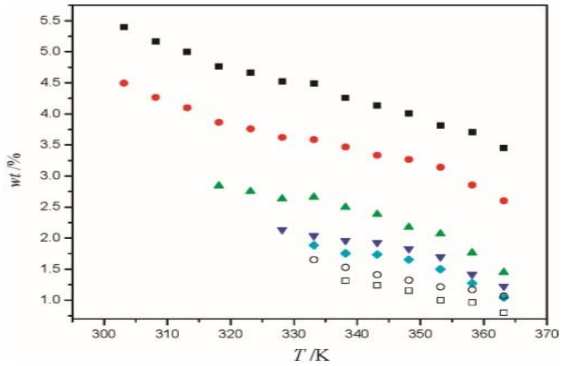

Figure 2.6: Solubility of hydrogen sulfide in different ratios of CPL:TBABr: ■, 1:1; ●, 2:1; ▲, 3:1; ▼, 4:1; ◆, 5:1; o, 6:1; □, 7:1. [34]

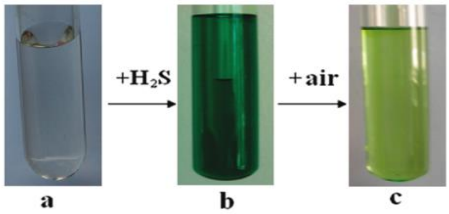

Figure 2.7: Color changes of systems a) DES, b) DES+H_2S, and c) DES+Air [34]

Particularly, the authors determined that solubility of H_2S in DES (caprolactam + tetrabutylammonium bromide) was 1.58 H_2S/kg DES at room condition (298K, 1 atm). Further from Figure 2.7, it can be seen that the DES was colorless initially, and it becomes bluish-green after absorption of H_2S. After that, when bubbled with air, the color changes to yellow green [34].

More recently, Liu et al., studied DES composed of choline chloride and urea, for absorption of H_2S, CO_2, CH_4 and found that the DES at 1:1.5 molar ratio of the constituent components have solubility of 0.39 H_2S/kg DES for hydrogen sulfide, 1.5 % for carbon dioxide, and 0.1 % for methane at 298 K, 1 atm [35]. The effect on solubility of H_2S in DES composed of choline chloride and urea is illustrated in Figure 2.8 [35].

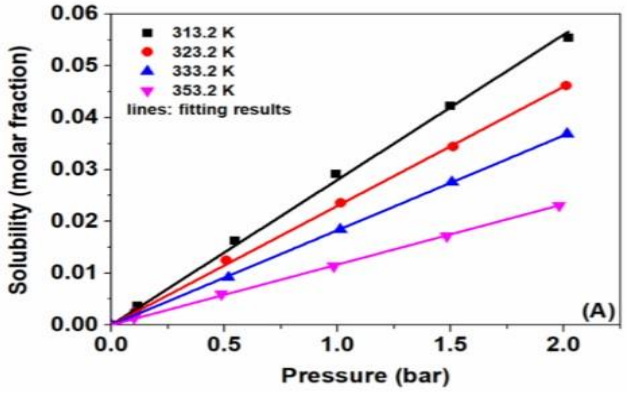

Figure 2.8: Solubility of hydrogen sulfide in the choline chloride based DES [35]**.**

In addition, the absorption of pure hydrogen sulfide through a combination of choline chloride and urea, as the DES is governed by the hydrogen bond interaction between chlorine of choline chloride and hydrogen of hydrogen sulfide. In general, the DES composed of choline chloride and urea demonstrated high selectivity and easy regeneration for absorption of pure hydrogen sulfide [35]. Further, Wu et al. synthesized carboxylic acid based DESs, for example, Pro/TBABr (1:1), Ac/TBABr (1:1), For/TBABr (1:1), ChCl/Pro (1:2), ChCl/Ac (1:2), ChCl/For (1:2) to absorb pure hydrogen sulfide at 298-318 K and 0.1-0.6 MPa. So, from various carboxylic acid based DESs, Ac/TBABr (1:1) and For/TBABr (1:1) showed good solubility for hydrogen sulfide around 1.25 mol H_2S/kg DES and 1.25 mol H_2S/kg DES respectively (Table A.1) [36]. In contrast, ChCl/Urea (1:1.5) showed relatively low capacity of H_2S, some carboxylic acid based DESs such as For/TBABr(1:1), ChCl/For(1:2), ChCl/Ac(1:2), and ChCl/Pro(1:2) illustrates moderate capacity for H_2S. But the solubility's of H_2S in CPL/TBABr (1:1), Pro/TBABr(1:1), and Ac/TBABr(1:1) were impressively high with 1.58 mol H_2S/kg DES, 1.66 mol H_2S/kg DES, 1.25 mol H_2S/kg DES respectively [36]. Consequently, it is clear that the DESs such as CPL/TBABr (1:1), Pro/TBABr(1:1), and Ac/TBABr(1:1) are preferable over many other DESs listed in Table A1, since they exhibited higher solubility values. Also, it means that DESs can be suitable

alternatives for absorption of H_2S. In summary, we observe from all of the above mentioned studies that DESs have great potential in absorption of H_2S and that different parameters such as operating temperature, pressure, DES composition had an effect on solubility efficiency. Certain reports show that with an increase of temperature, the solubility efficiency decreases, however, the low pressure is suitable for the absorption of H_2S process.

Shah, Mansurov, and Mjalli earlier research work studied the mixture of reline (ChCl:Urea, 1:2 molar ratio) with dimethylsulfoxide (DMSO) via the MD simulations [14]. The authors reported that the DMSO have a very limited effect on choline-urea, chlorine-urea, and urea-urea interaction energies in terms of hydrogen bonding [7], [14]. Moreover, Liu and his research team performed DFT study and MD simulations for ChCl:Urea (1:2 molar ratio) in the presence of H_2S, and then noted that the chlorine is major site for interaction with H_2S [35].

The H_2S solubility in the DESs is compared with ILs as shown in Table A.1. Namely, phenolic protic ILs and hydrophobic protic ILs illustrated high absorption capacity for H_2S, while other ILs showed the same H_2S absorption capacity as DESs. However, the DESs are preferable over ILs, since DESs are biodegradable, non-flammable, have low vapor pressure, and also low cost, which makes them very promising, and additional advantage over ILs, in large scale applications [16]. While experiments highlight effectiveness of these DESs, however, the mechanism of absorption and their functioning remains obscured. Moreover, the previous studies are based on pure H_2S and not in the competing environment of natural gas. Alongside, the existing literature covers only experimental studies on absorption of pure H_2S using DES and does not explore modeling and simulations of the topic. Considering these, we herein perform ab-initio and molecular simulations, for first time, to 1) explore the mechanism of formation of these novel DESs, 2) analyze the process of absorption at molecular level, 3) determine the effect of process parameter on the absorption capacity, and 4) determine the performance of these DESs in competitive environment of natural gas. The target of this work is also to provide rational guidelines, based on the understanding the desulfurization mechanism by analyzing the results of ab-initio and molecular dynamic simulation for the various systems DES with H_2S and CH_4, for better design of DESs.

Chapter 3 – Materials and Methods

3.1 Ab-initio calculations

The computational chemistry software's are primarily based on various quantum methods to solve the Schrodinger equation. The Schrodinger equation is the basis of quantum mechanics (QM) to calculate the ground state geometry (equation 1).

$$H \times \psi = E \times \psi \qquad (1)$$

In the above equation, H is the Hamiltonian operator, ψ is the wave function, E is the energy. Critically important point of QM is that in classical systems, Hamiltonian operator behaves quite differently than an equivalent function. The exact solution of Schrodinger equation produces yields energy and wave function which is giving complete explanation of the electronic properties. However, it is impossible to solve Schrodinger equation exactly except for simple problems. Considering these, there are different quantum-chemistry methods to solve Schrodinger equations.

Density Functional Theory (DFT) methods are generally implemented in computational chemistry and primarily based on approximate solutions of the Schrodinger equation. In DFT, probability of finding electron is implemented to solve Schrodinger equation rather than a mere wave function which was introduced by P Hohenberg and W Kohn in 1964. Further next, it is sufficient to know the electrons density which greatly reduced the degree of freedom and lead to simple computational study of large molecular systems. Hohenberg and Kohn (HK) reported that the total energy of a system of electrons in an external potential is known exactly as a function of the electronic density. Basically, Hohenberg and Kohn (HK) showed that the ground-state density is a density that minimizes total energy. Kohn-Sham method is the fundamental of most Density Functional Theory calculations.

3.2. Molecular Dynamics simulations

Molecular Dynamics (MD) simulation is a computational method implemented to implement molecular interaction and movements.

Table 3.1: Equations for MD simulation

#	Equations:
3.1	$f_i = -\nabla_n \times U(r) = m_i \times \frac{d^2(r_i)}{dt^2}$
3.2	$H = K + U(r)$
3.3	$K = \sum_{i=1}^{N} \frac{m_i \times v_i^2}{2}$
3.4	$U(r) = U_{bond} + U_{angle} + U_{UB} + U_{dihedral} + U_{improper} + U_{LJ} + U_C$
3.5	$U_{bonds} = \sum_{bonds} K_b(b - b_0)^2$
3.6	$U_{angle} = \sum_{angles} K_\theta(\theta - \theta_0)^2$
3.7	$U_{UB} = \sum_{UBs} K_s(s - s_0)^2$
3.8	$U_{dihedrals} = K_\varphi(1 + \cos(n\varphi - \delta))$
3.9	$U_{improper} = \sum_{impropers} K_\omega(\omega - \omega_0)^2$
3.10	$U_{LJ} = \sum_{nonbonded\ pairs} \epsilon_{ij}((\frac{r_{ij}^{min}}{r_{ij}})^{12} - 2(\frac{r_{ij}^{min}}{r_{ij}})^6)$
3.11	$U_C = \sum_{nonbonded\ pairs} \frac{q_i q_j}{4\pi\epsilon_0\epsilon_r r_{ij}}$

Namely, the molecular dynamics obeys the Newton's laws of motion due to potential energy (U(r)), which derive from intermolecular interaction as can be seen from equation 3.1. The total energy (H) of the designed system containing N molecules is comprised of potential energies (U(r)) and kinetic energies (equation 3.2, 3.3 and 3.4). Meanwhile, U_{bond} is the energy which stored in covalent bonds in the system. Every bond is characterized by a harmonic spring with specific actual bond length (b), force constant (K_b), and the equilibrium length bond b_0 as illustrated on equation 3.5. In addition, U_{angle} is valence angle energy which is characterized by the angle

between two covalent bonds (θ, θ_0)and angle force constant (K_θ) (equation 3.6). The next term U_{UB} (Urey-Bradley component, equation 3.7) is a cross-term account for atoms experiencing nonbonding interactions, where s_0 is the distance of equilibrium, s is the distance between separate atoms, K_s is the force constant. The following term $U_{dihedral}$ is the energy of the dihedral interaction which is consists of multiplicity factor of the variable n, angle of the dihedral φ, dihedral force constant K_φ, and phase δ as shown on figure 3.8. Another term $U_{improper}$ is the improper energy for out of plane torsions, where the out of plane angle is ω-ω0, and force constant is K_ω as shown on equation 3.9. The remaining terms U_{LJ} is Lennard-Jones potential which is modeling Van der Waals interactions, and U_c is Coulombic potential, which is responsible for electrostatic interactions as shown on the equations 3.10 and 3.11.

3.2 Computational details

GROMACS with Visualization Molecular Dynamics (VMD), was implemented for molecular dynamics simulation to calculate interaction energies, hydrogen bonding, radial distribution function and other properties of modeled system (Figure 3.1 a). A mixture of hydrogen sulfide (H_2S) and methane (CH_4) was taken as representative model of natural gas. The optimized forcefield and coordinate parameters (dihedrals, bond, angle, partial charges) for tetrabutylammonium ion (TBA), bromide ion, chloride ion, caprolactam (CPL), urea, choline ion, monoethanolamine (MEA), methyltriphenylphosphonium bromide (MTPPBr), methane (CH_4), and hydrogen sulfide (H_2S) was taken from ATB (Automated Topology Builder) database and LJ (Lennard-Jones) parameters was obtained from the standard gromos forcefield [21].

MD simulations were started through creating a low density box with the $10 \times 10 \times 10$ nm^3 dimensions and inserting number of molecules according to Table 3.2. The gromos54a7 force field was implemented in this study. To be more specific, energy minimization was performed with a maximum force constraint of less than 1000 kJ/mol/nm on any atom to optimize the initial box configuration. After minimization of energy, NVT and NPT were simulated at 298 K temperature and 1 bar pressure for 0.1 ns each. Eventually, MD run was performed for 10 ns. LINCS constraint algorithm was used for all bonds during the simulation. 1.5 nm cut-off was used for LJ and Coulombic interactions. Long-range interactions were computed with 0.16 nm grid spacing and fourth-order interpolation [8], [13]. V-rescale method was used to maintain temperature and

Parrinello-Rahman coupling was implemented to maintain system pressure [4], [37], [38]. Additionally, MD simulations were performed by using periodic boundary conditions in all directions.

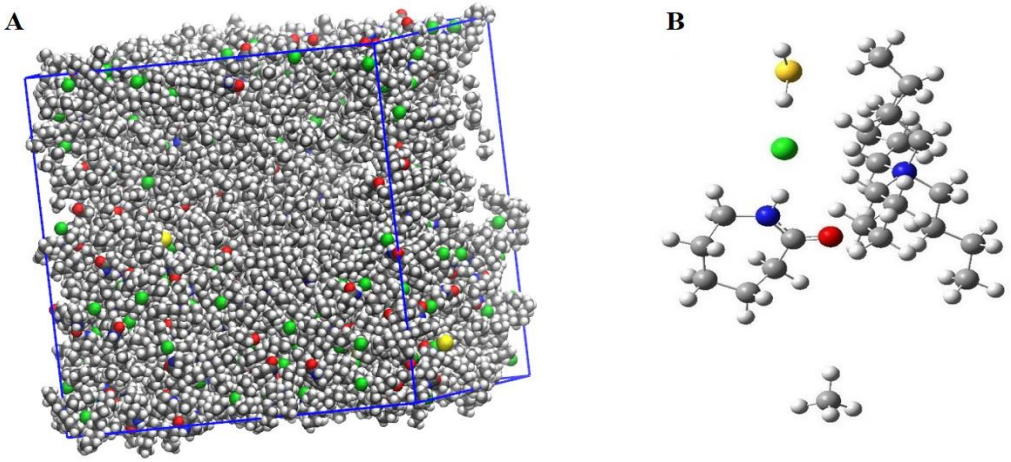

Figure 3.1: Designed system DES (CPL:TBACl)+H_2S+CH_4 in (a) Gromacs, and (b) Gaussian16. Color key: white: hydrogen; grey: carbon; blue: nitrogen; yellow: sulfur; green: chloride.

Initially, MD simulations were performed on the individual components of the DES; pure TBABr and pure CPL for reference. Further next, the desulfurization of natural gas was studied by mixing modeled natural gas and DES at different temperature and pressure. Then, a combination of CPL and TBABr (see table 3.2; system 1, 1:1 mole ratio) was simulated to explore intermolecular interactions within the DES (Figure 3.1a). Next, a mixture of hydrogen sulfide (H_2S) and methane (CH_4) was taken as representative model of natural gas and was simulated (see table 3.2; system 2 and 3). Mainly, 5000 ppm H_2S was selected, using 1 molecule of H_2S and 200 of CH_4 (see table 3.2; system 2). Moreover, as highlighted in footnote a, system 2 was also simulated at 10000 ppm of H_2S to explore the effect of H_2S concentration on natural gas sweetening. Moreover, in table 3.2; system 3 with more number of H_2S and CH_4 molecules was created to later explore the effect of model fuel:DES mole ratio on desulfurization of natural gas. Next, systems 4 and 5 were simulated to investigate natural gas sweetening implementing CPL:TBABr based DES.

Secondly, a mixture of CPL:TBACl, (see table 3.2; system 7) at 1:1 molar ratio, as the

DESs, was simulated to study the intermolecular interactions within the DES. Meanwhile, CPL:TBABr is investigated in the experiments, as mentioned in Chapter 2, simulations with CPL:TBACl were also studied to compare, as TBACl has been commonly used earlier, in several experiments and simulations [11], [21], [22]. Next, system 7 and 8 were simulated next, i) to investigate natural gas sweetening by the CPL:TBACl based DES, ii) to explore the effect of H_2S concentrations on desulfurization efficiency (5000/10000 ppm, as noted in the footnote a), iii) study the effect on fuel:DES ratio and iv) to understand the effect of process parameters (temperature and pressure) on the process (see footnote b). Finally, system 9 and 10 were simulated to compare H_2S absorption efficiency of two other DESs, namely ChCl:Urea, and MTPPBr:MEA. These DESs were used based on their common usage in the literature [25], [29], [30].

Table 3.2: The designed systems details along with the number of molecules that will be used to explore natural gas sweetening by the DESs at 298 K and 1 bar.

#	**CPL**	**TBABr**	**H_2S**	**CH_4**
1	400	400	-	-
2	-	-	1	200
3	-	-	5	1000
4	400	400	1	200
5	400	400	5	1000
	CPL	**TBACl**	**H_2S**	**CH_4**
6	400	400	-	-
7	400	400	1	200
8	400	400	5	1000
	ChCl	**Urea**	**H_2S**	**CH_4**
9	500	1000	5	1000
	MTPPBr	**MEA**	**H_2S**	**CH_4**
10	400	2400	5	1000

[a]System 2 and 7 were also simulated with 2 H_2S & 200 CH_4, while system 3 and 8 were created with 10 H_2S with 1000 CH_4 molecules (10000 ppm). [b]System 8 with 5 H_2S was also simulated at 1 bar 333 K, and 10 bar 298 K to investigate the effect of temperature and pressure on desulfurization of natural gas.

GAUSSIAN16 with GaussView (v 6.0), was implemented for ab-initio simulation to optimize the ground state geometries. The optimized geometries of CPL and TBACl was obtained from the Automated Topology Builder (ATB) server and implemented in our study [39]. Electronic ground state geometries for CPL, TBACl, their mixture as the DES, and the DES + H_2S + CH_4 in the gas phase were optimized via the implementation of B3LYP DFT methods, and 6-311++G(d,p) basis set (Figure 3.1b). Meanwhile, B3LYP DFT method and 6-311++G(d,p) basis set was selected considering its well performances for a broad range of various ILs and DESs according to the previous computational studies [40]–[44]. By analytical calculation of the second energy derivatives, all stationary points were confirmed to be true minima on their respective potential energy surfaces. The thermal corrections at 298 K and 1 atm were computed in order to obtain the Gibbs free energy and enthalpy values. The total electronic energies (ΔE), the total electronic energies corrected with zero-point energies ($\Delta(E+ZPE)$), enthalpies (ΔH), and Gibbs free energies (ΔG) were calculated on the bases of obtained results from electronic ground state geometry optimizations in gas phase.

3.3 Validation of forcefield parameters

The densities and diffusion coefficients of gases and liquids will be computed through molecular dynamics simulations and then compared with experimental values. The good agreement between theoretically computed and experimental value validates that our molecular dynamic simulation model is correct. The choice of force-field parameters effects on the results of molecular dynamic simulation and hence validation is essential to compare results with the experiments. In this regard, gromos54a7 force field was applied in our study. Consequently, densities and diffusion coefficients of liquids and gases were simulated and compared with experimental values. Initially, MD simulations were performed on the individual components of the model natural gas; pure hydrogen sulfide and pure methane for obtaining its density and self-diffusion coefficient to compare with experimental values. In this regard, computed and literature densities of methane, and hydrogen sulfide are in good agreement as shown on Table 3.3. In addition, the self-diffusion coefficients of methane and hydrogen were observed from the simulations to be 0.119 cm^2/s and 0.110 cm^2/s, in comparison to 0.24 cm^2/s and 0.200 cm^2/s, as noted in the literature [45], [46]. Moreover, densities of the two DESs including ChCl:Urea and MTPPBr:MEA were in close agreement with the experimental value (see table 3.3) [14], [47].

Moreover, we obtained the density of CPL:TBABr and CPL:TBACl to be 1096 kg/m^3 and 1067 kg/m^3 from the simulations, however, it could not be verified from the literature, as no experiments have been reported. Taken together, it can be concluded that densities from literature and gromacs simulation are in good agreement which validate model by supports choice of force-field parameters.

Table 3.3: Theoretically computed and literature values of densities.

Components	Density (kg/m^3)	
	Computed	Literature
CH_4	0.84	0.65 [45]
H_2S	1.48	1.39 [46]
ChCl:Urea (1:2)	1180	1194 [14]
MTPPBr:MEA (1:6)	1164	1107 [47]

Chapter 4 – Results and Discussion

4.1 Deep Eutectic Solvents formation

The molecular mechanism of the Deep Eutectic Solvent formation is studied for a combination of caprolactam and tetrabutyl ammonium halides. The primary aim of this work is to investigate the formation of caprolactam based DESs, to understand the observed strong depression in the melting point through molecular dynamic simulations.

Considering this, we investigated CPL:TBABr and CPL:TBACl designed systems in terms of their intermolecular interaction energies, radial distribution functions (rdfs), and number of hydrogen bonds using molecular dynamic simulations. The interaction energies were calculated by summing short-range Lennar-Jones and short-range Coulomb potential for various pair of molecules. Next, we firstly explored CPL:TBABr system, as the caprolactam based DES. The interaction energy between TBA ion and Br ion (pure TBABr, 400 molecules) was reached to be –21286.0 kJ/mol, highlighting strong ionic interactions (see figure 4.1A). However, the ionic interaction energy between the TBA ion and Br ion declined to –18311.41 kJ/mol after mixing the pure TBABr with pure CPL (see table 3.2; system 1). The simulation results reveal weakening of ionic interactions between the TBA and Br ions, which explains the strong depression in the melting point as noted during the formation of the caprolactam based DES through molecular dynamic simulations.

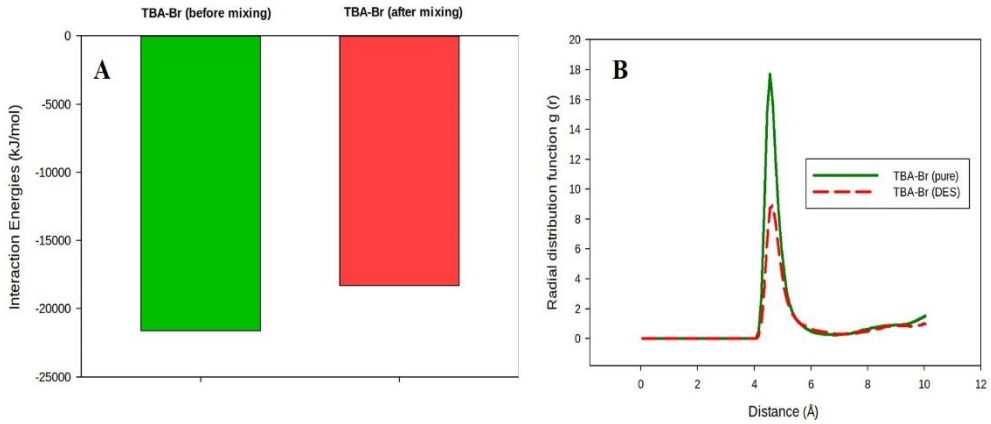

Figure 4.1: A) Interaction energy between TBA ion and Br ion for pure TBABr and system 1 (DES), B) Rdfs between TBA ion and Br ion in pure TBABr and in system 1 (DES).

In the next analysis, we start with comparing simulation of pure TBABr with the system

containing CPL:TBABr (1:1 molar ratio), as the DES (system 1) using rdfs. The radial distribution functions (rdfs) between TBA ion and Br ion were shown on Figure 4.1B. The rdfs illustrate the measure of probability for an atom being at the distance r from the reference atom. Central nitrogen atom of the TBA ion was chosen as reference to determine the rdfs.

The rdfs between the nitrogen atom of the TBA ion with bromide ion before and after mixing with CPL (system 1) are shown on Figure 4.1B. From this figure, it can be clear that in pure TBABr, the first peak appears at distance of 4.35 Å with peak value of rdfs is 16.7. Although, in the DES (system 1), the interaction between TBA and bromide ion decreased significantly as shown in rdfs with peak value of ~9. Interestingly, this could be explained through the fact that TBA ion started to interact with CPL molecule, as also highlighted from the next Figure 4.2A.

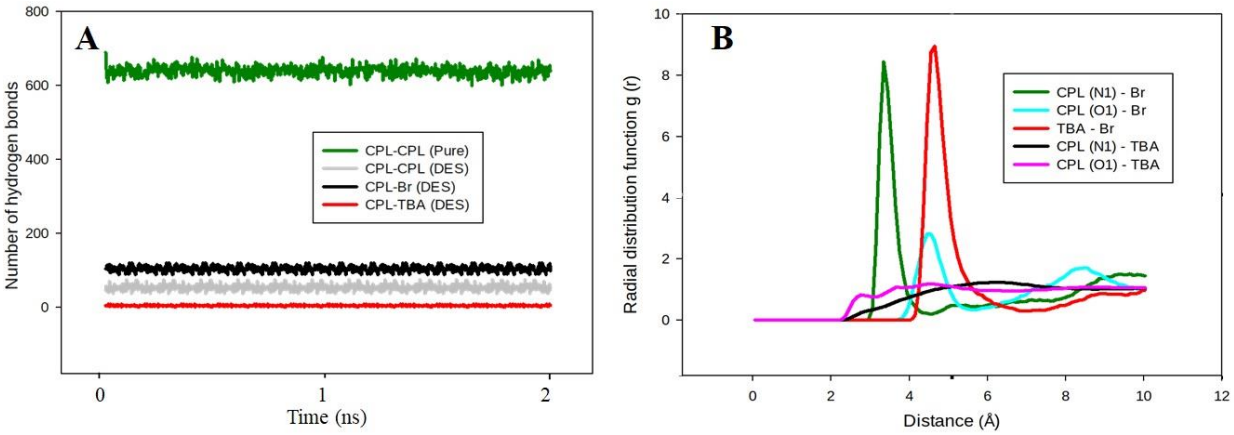

Figure 4.2: A) Number of H-bonding between CPL molecules before and after mixing with TBABr, B) Rdfs between TBA, CPL, and Br in DES.

In general, the formation of DESs is explained through the presence of hydrogen bond interactions in DES between hydrogen bond acceptor and hydrogen bond donor [20]. Hence, as shown in Figure 4.2 A, the number of H-bonding between CPL molecules was 638±7 in pure caprolactam. However, the number of hydrogen bonding between CPL molecules drops significantly to 52±3 (CPL:TBABr), after mixing with TBABr, implying a further weakening in the intermolecular interactions between CPL molecules. Interestingly, there were observed strong interactions between CPL molecules and Br ions in the caprolactam based DES, as the number of H-bonds between CPL molecule and Br ion was 103±8 (CPL:TBABr). Meanwhile, few numbers of hydrogen bonds were noted between CPL molecule and TBA ion, revealing weakening on intermolecular interactions between them. Further next, rdfs between the constituent components

(CPL, TBA, and Br) of the DES were illustrated in Figure 4.2B. CPL might have interacted with Br ion using its nitrogen or oxygen atom and hence rdfs were plotted with respect to both atoms. The first peak for nitrogen atom of CPL molecule and Br ion had a peak value of 8.2 in the CPL:TBABr, as the DES (system 1), meanwhile, the peak value is 2.1 in the rdfs between oxygen atom of CPL molecule and Br ion, suggesting N atom of CPL plays critically important role to hydrogen bonding with Br ion. Next, rdfs between TBA/Br showed the highest peak value of ~9. However the peak between TBA/Br was higher than CPL/Br. The low peak value was observed for rdfs between CPL(N)/TBA(N), and CPL(N)/TBA(N), meaning that the CPL molecule does not interact with TBA ion. To sum up, a sharp decrease noted in the number of H-bonds between CPL leads to the formation of DES by hydrogen bonding of CPL with bromide ion (CPL:TBABr), while weakly interacting with TBA ion.

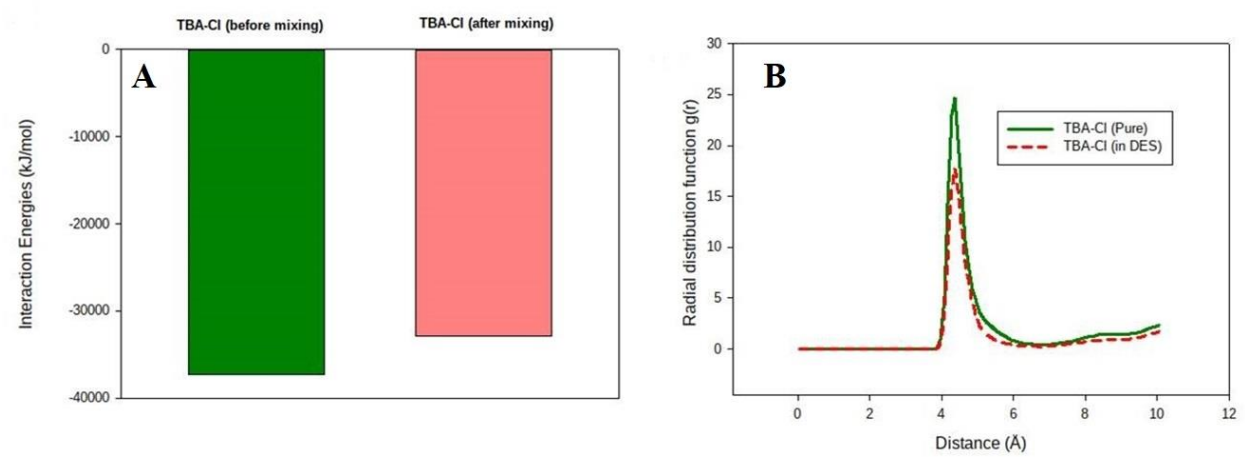

Figure 4.3: A) Interaction energy between TBA ion and Cl ion, B) Rdfs between TBA ion and Cl ion for in pure TBACl and in system 1 (DES).

After that, the mixture of CPL:TBACl (1:1 molar ratio), as the DES was investigated (system 6). The results reveal that interaction energy between TBA and Cl ion before mixing (pure TBACl, –37271.95 kJ/mol) is greater than the after mixing with CPL (in the DES, –32839.05 kJ/mol), which show the weakening of interactions (Figure 4.3A). While the decline in the case of Br ion was ~15%, in the case with Cl ion was ~12%. In addition, the rdfs between the nitrogen atom of the TBA ion with chloride ion before and after mixing with CPL (system 6) are shown on Figure 4.3B. From this figure, it can be clear that in pure TBACl, the first Cl ions appears at distance of 4.35 Å from the nitrogen atom of the TBA ion and the peak value of rdfs is 24.68. Although, in DES (system 6), the interaction between TBA and chloride ion decreased

significantly, as the peak value of 18.

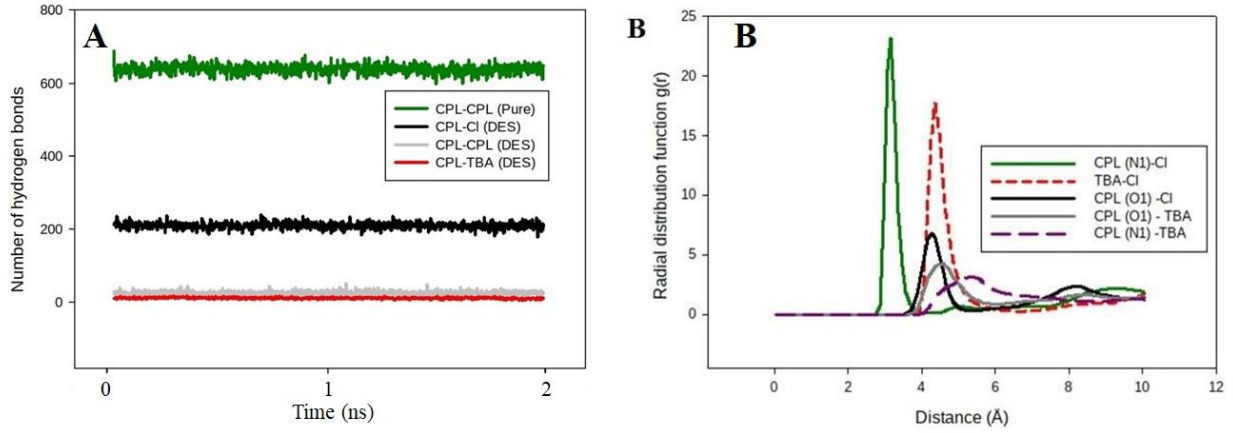

Figure 4.4: A) Number of H-bonding between CPL molecules before and after mixing with TBACl, B) Rdfs between TBA, CPL, and Cl in DES.

Furthermore, as shown in Figure 4.4A, the number of H-bonding between CPL molecules was 638±7 in pure caprolactam. However, the number of hydrogen bonding between CPL molecules drops significantly to 11 (CPL:TBACl), after mixing TBACl. In addition, the number of H-bonds between the chloride ion and CPL molecule was 210±5 (CPL:TBACl). In addition, no hydrogen bonds between CPL/TBA were noted in the DES (system 6). The rdfs between TBA, CPL and chloride ions are shown on Figure 4.4B. The results reveal that the CPL ion started strongly to interact with chloride ion. It is also crucial to highlight that the weakening in the strength of interactions between the TBA and Cl ions causes the strong depression the melting point of the DES. The same results were obtained for the formation of DES from CPL:TBABr (at a mole ratio 1:1).

Further next, ab-initio calculations were performed on CPL:TBACl to analyze the formation mechanism of DES. Each constituents of DES (CPL and TBACl) were optimized separately as an initial step of the DFT study. After geometry optimizing each CPL and TBACl structures, a combination of CPL and TBACl (1:1, mole ratio) as the DES structure was proposed and optimized. For this purpose, the theoretically stable conformers of CPL, TBACl, and DES geometries were optimized by applying density functional theory (DFT), B3LYP 6-331++G(d,p) level of theory in the gas phase. This level of theory has been selected based on previous studies, which was proven successfully for ILs, natural-DES, and DES. The analysis of the excess energies,

optimized geometries, molecular electrostatic maps, and molecular orbital's were determined to study the formation of the caprolactam based DES.

The quantum chemical relative energy calculations for optimized conformers of CPL, TBACl, and DES in the gas phase are shown in Table 4.1. The *"Excess energy"* (ΔE_{excess}) was defined using the difference between the total energy values of DES and constituent components (equation 1).

$$\Delta E_{excess} = E_{DES} - (E_{pure\ CPL} + E_{pure\ TBACl}) \quad (1)$$

A low value of ΔE_{excess}, as observed in table 4.1, suggests low melting point of the DES. The calculated total energies of the caprolactam based DES system is lower by -64.84 kJ/mol in comparison to the sum of the total energies of individual optimized geometries of caprolactam and tetrabutyl ammonium chloride. That indicates that there are contributions of non-covalent interactions to the caprolactam based DES stability as can be seen from Table 4.1. The same trends were observed for the electronic energy (–73.77 kJ/mol), electronic energy+ZPE, electronic energy (–69.83 kJ/mol), ΔH (–68.78), ΔG (–22.57kJ/mol).

Table 4.1: Thermochemistry for electronic ground state of CPL, TBACl and DES at DFT B3LYP 6-311++G(d,p) level

Energy (kJ/mol)	**CPL**	**TBACl**	**DES**	**ΔE_{excess}**
Total Energy	–958807.13	–3008903.07	–3967775.06	–64.84
Electronic Energy	–959269.22	–3010291.44	–3969634.43	–73.77
Electronic energy + ZPE	–958826.82	–3008970.02	–3967866.69	–69.83
ΔH	–958804.76	–3008899.14	–3967772.69	–68.78
ΔG	–958910.31	–3009124.40	–3968057.30	–22.57

To understand further insights into the interactions between the constituent components of the DES, the most stable gas phase geometries of the CPL, TBACl and DES (CPL:TBACl at 1:1 mole ratio) were illustrated in Figure 4.5A. As given, the chloride is hydrogen bonded to the central nitrogen atom of the amide functional group by 2.224 Å. The central oxygen atom of caprolactam is closer to the tetrabutyl ammonium ion by 2.273 Å. The trend is in agreement with the results

obtained from the MD simulations. Molecular electrostatic maps reveal an effective visualization of polarity and charge distribution of the investigated CPL, TBACl, and DES structures. The plots were shown in Figure 4.5B. Close view of these isosurfaces provide that the chloride ion of tetrabutylammonium chloride and oxygen atom of caprolactam before and after mixing is covered with red or negatively charged isosurfaces corresponding to aggregation of electron density. As observed in the DES case, the chlorine ion of tetrabutylammonium chloride can be more delocalize by amine group, and form intermolecular hydrogen bonding which results in less negative charge on chloride ion.

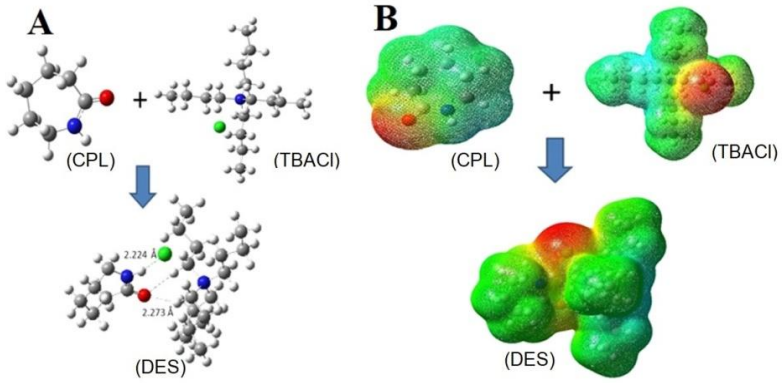

Figure 4.5: A) Optimized structures and B) Molecular electrostatic maps for CPL, TBACl and DES in the gas phase.

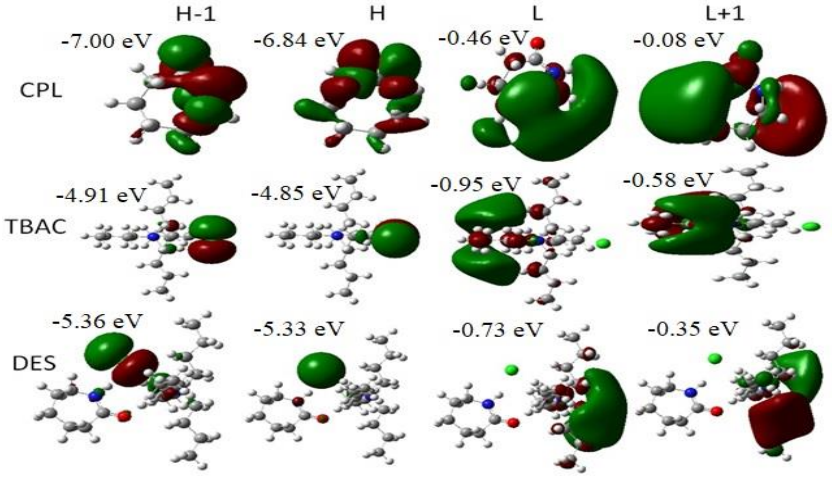

Figure 4.6: Representations (isovalue=0.02, isodensity=0.0004) of H-1, H, L, L+1 MOs density for optimized electronic ground state geometries of CPL, TBACl, and DES.

The *L+1, L, H, H-1* molecular orbital densities representations for CPL, TBACl, and DES were provided in Figure 4.6. In general, it can be seen that LUMO is always formed around the

TBACl and HOMO formed around the chloride ion. HOMO-LUMO gap is related to the stability and the reactivity of the studied CPL, TBACl, and DES. In this regard, it could be highlighted that higher molecular stability and lower chemical reactivity for larger value of computed HOMO-LUMO gap (−4.6 eV) for the DES.

4.2 Desulfurization of Natural Gas

After studying formation of the caprolactam based DESs, we performed molecular dynamics simulations along with model natural gas. We began to investigate the interaction energies between H_2S and CH_4 in the modeled natural gas.

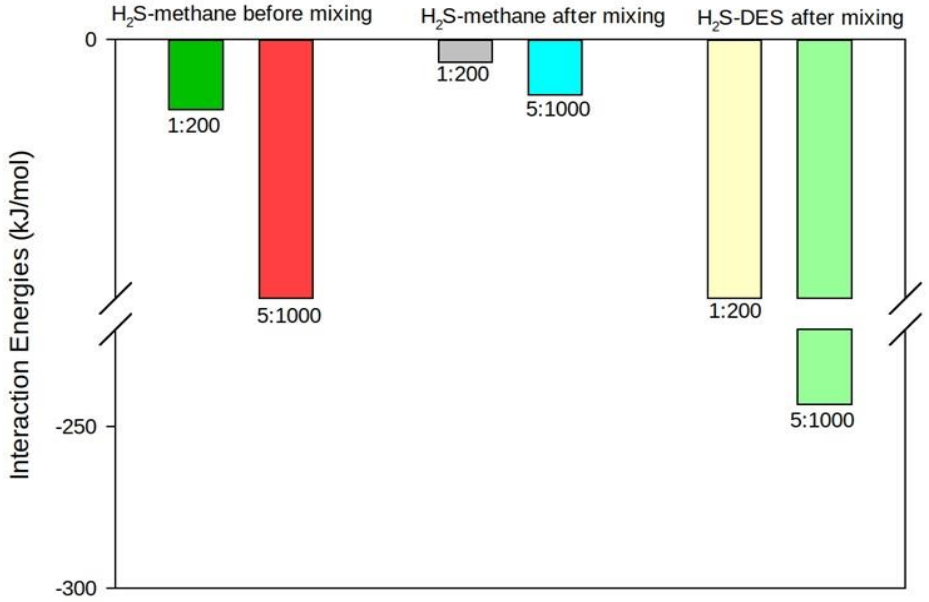

Figure 4.7: Interaction energy between CH_4/H_2S before and after with DES and H_2S/DES.

Running systems 2 and 3, it was observed that the interaction between CH_4/H_2S is significantly high (–0.99 kJ/mol for system 2, and −1.54 kJ/mol for system 3), which means that efficient natural gas sweetening must be able to absorb H_2S from the natural gas (Figure 4.7). However, the interaction energy between H_2S/CH_4 after mixing with DES (CPL:TBABr) was –0.21 kJ/mol, and –6.24 kJ/mol for system 4 and 5, respectively as shown on Figure 4.7. The obtained results reveal that the molecular interactions between H_2S and CH_4 were weakening in the presence of DESs (CPL:TBABr). In addition, the interaction energy between H_2S and CH_4 declined by ~five-fold for 1:2 fuel:DES mole ratio, however, it increases by ~four-fold for 2.5:1

fuel:DES ratio. While, high interaction energies between H_2S/DES were noted at both (1:2 and 1.25:1) the fuel:DES ratios (–42.39 kJ/mol for system 4 and –243.22 kJ/mol for system 5), suggesting that the DES captures H_2S molecules from the natural gas. However, the CPL:TBABr, as the DES is more efficient at low natural gas amounts.

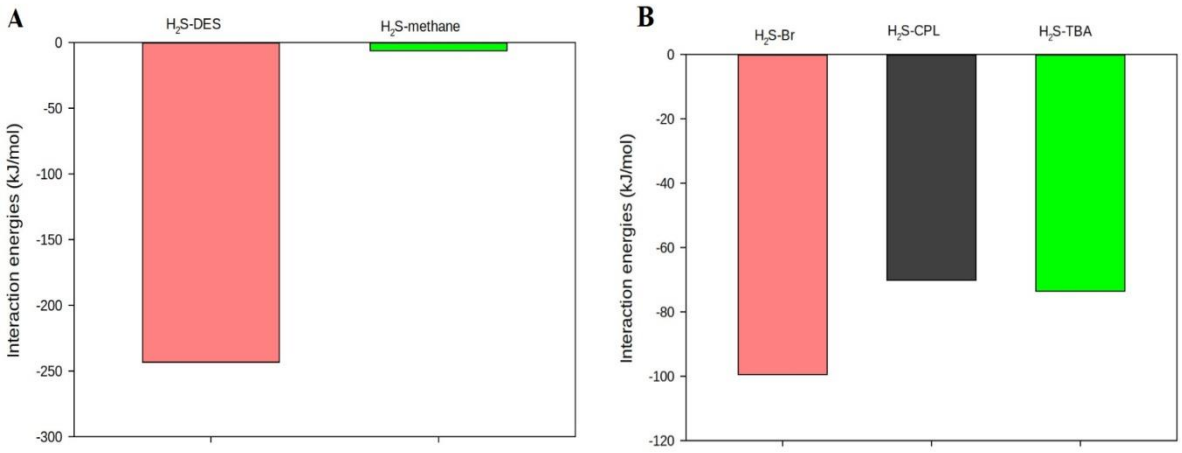

Figure 4.8: Interaction energies between A) H_2S-DES, H_2S-Methane, B) H_2S-DES components.

Analyzing Figure 4.8A and B, it can be highlighted that interaction energy between H_2S and CH_4 was –6.24 kJ/mol in the presence of DES (CPL:TBABr, 1:1, mole ratio) indicating a weakening of intermolecular interactions between H_2S and CH_4 molecules. On the other hand, strong molecular interactions between DES and H_2S were observed with energy of –243.22 kJ/mol. Particularly for CPL:TBABr (1:1, mole ratio) DES system, the interaction energy between Br ion and H_2S molecule (–99.45 kJ/mol) was higher in comparison with the interaction energies of CPL/H_2S (–70.13 kJ/mol) and H_2S/TBA ion (–73.65 kJ/mol) as shown in Figure 4.8B. Consequently, it can be concluded that molecular interactions between H_2S and Br ion are the stronger in CPL:TBABr, as the DES.

Next, rdfs between H_2S and the components of the DES were calculated and compared with H_2S/CH_4 for system 5 (Figure 4.9A). The sulfur (S) atom of H_2S, nitrogen (N) atom of TBA ion and CPL molecule were implemented. The results reveal that the rdf between H_2S/Br has the highest peak value of 9.6, at a distance of 3.9 Å, indicating a strong hydrogen bond interaction. Furthermore, rdfs of H_2S/TBA and H_2S/CPL have the peak marginally higher than for H_2S/CH_4, thereby favoring removal of H_2S from CH_4.

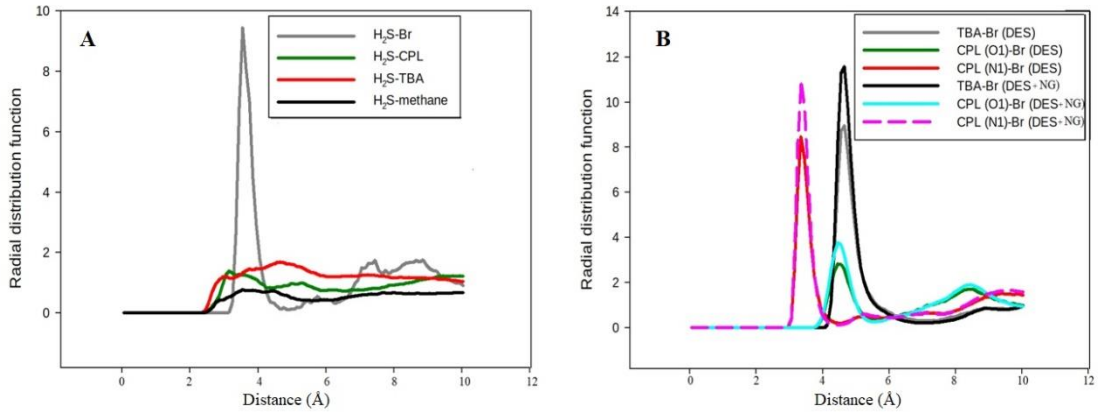

Figure 4.9: A) Rdfs between H_2S-CH_4 and other components of the DES in system 5, B) rdfs between the DES's components before (system 1) and after mixing with the natural gas (system 5).

One of the key-indicative of a good solvent is its regenerability after absorption. Mainly, molecular structure of DES should not change during absorption process for efficient regeneration. To this end, we further compare the rdfs of TBA/Br, CPL (O1)/Br, and CPL (N1)/Br before and after mixing of DES with model natural gas as shown in Figure 4.9B. The results reveal consistency of these rdfs which means stability of DES structure. Overall, the analysis indicates that molecular interactions between CPL:TBABr based DES largely remain the same after absorption of H_2S in the presence of CH_4 suggesting that the desulfurization does not noticeably affect the structure of these DES.

After studying desulfurization of natural gas using CPL:TBABr, as the DES, the molecular dynamics simulations were performed on mixture DES (CPL:TBACl) and natural gas as shown on systems 7 and 8. Figure 4.10A and B show the interaction energies for H_2S/CH_4, H_2S/DES, and H_2S/DES components before and after mixing DES with natural gas. The obtained results reveal that the molecular interactions between H_2S and CH_4 were weakening to be –10.77 kJ/mol in the presence of DESs (CPL:TBACl). Moreover, the DES captures H_2S molecules as the interaction energy of DES/H_2S was closer to –252.84 kJ/mol (CPL:TBACl). On the other hand, as shown in Figure 4.10A and B, the interaction energies of H_2S/DES components illustrates that chloride ions (–154.05 kJ/mol) are the critically important, while caprolactam (–51.89 kJ/mol) and

tetrabutylammonium ions (–49.90 kJ/mol) are second important DES components for desulfurization of natural gas.

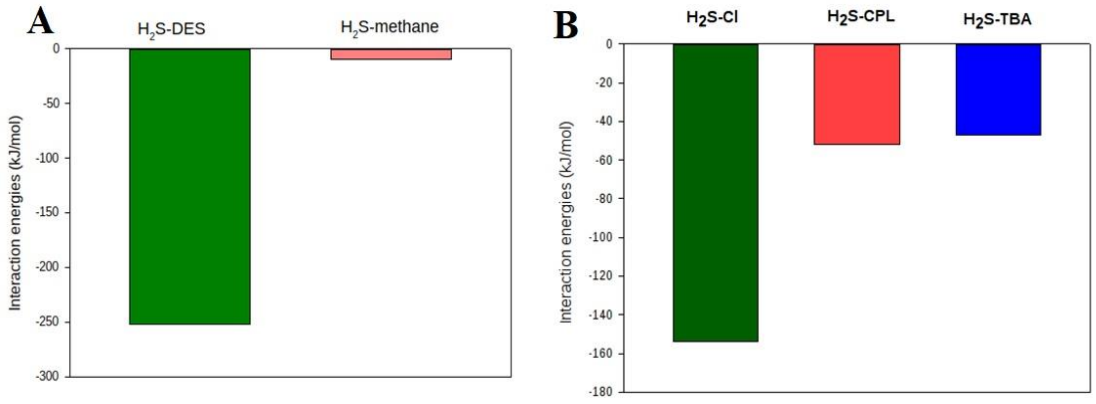

Figure 4.10: Interaction energies between A) H_2S-DES (CPL:TBACl), H_2S-Methane, B) H_2S-DES (CPL:TBACl) components.

To understand the DES (CPL:TBACl) + natural gas system, radial distribution functions were illustrated for H_2S molecules with DES components and methane as shown on Figure 4.11. It is clear that the results indicate that the H_2S weakly interacts with CH_4, but H_2S has strong interactions with Cl ions of CPL:TBACl, followed with caprolactam and tetrabutylammonium ions, which supports previous results. The radial distribution function results implies that (i) caprolactam molecules and tetrabutyl ammonium ions do not have direct interactions with H_2S, and are closer to H_2S because of DES structure, (ii) chloride ion was crucial component of DES for interaction with H_2S.

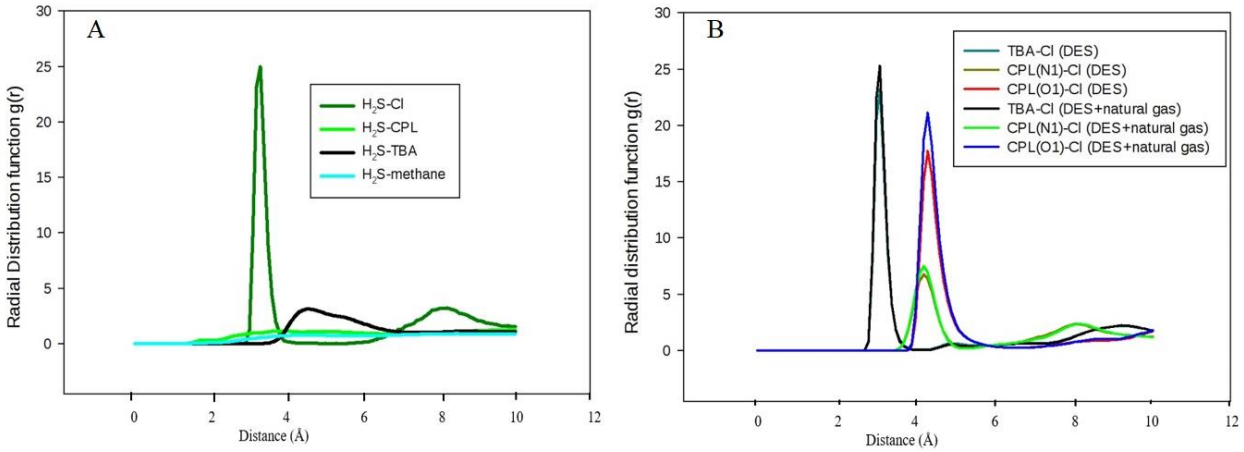

Figure 4.11: Rdfs for A) Hydrogen sulfide with methane and DES (CPL:TBACl) components B) DES (CPL:TBACl) before and after mixing with model natural gas.

In addition, coordination of DES components did not change after mixing with model natural gas as shown on Figure 4.12A and B, which means stability of DES structure. For instance, the number of H-bonding between CPL molecules and Cl ion was closer to 210±6 in CPL:TBACl. After mixing with natural gas, the number of hydrogen bonding between CPL molecules and chloride ions remained constant to 220±8. In addition, the number of H-bonds between the chloride ion and CPL molecule were also constant after mixing with natural gas. A consistence in the number of H-bonds between DES components before and after mixing with DES means their stability and reusability. The Figure 4.12B illustrates the visual representation of natural gas sweetening process, where after molecular dynamic simulation, hydrogen sulfide molecules was absorbed by DES.

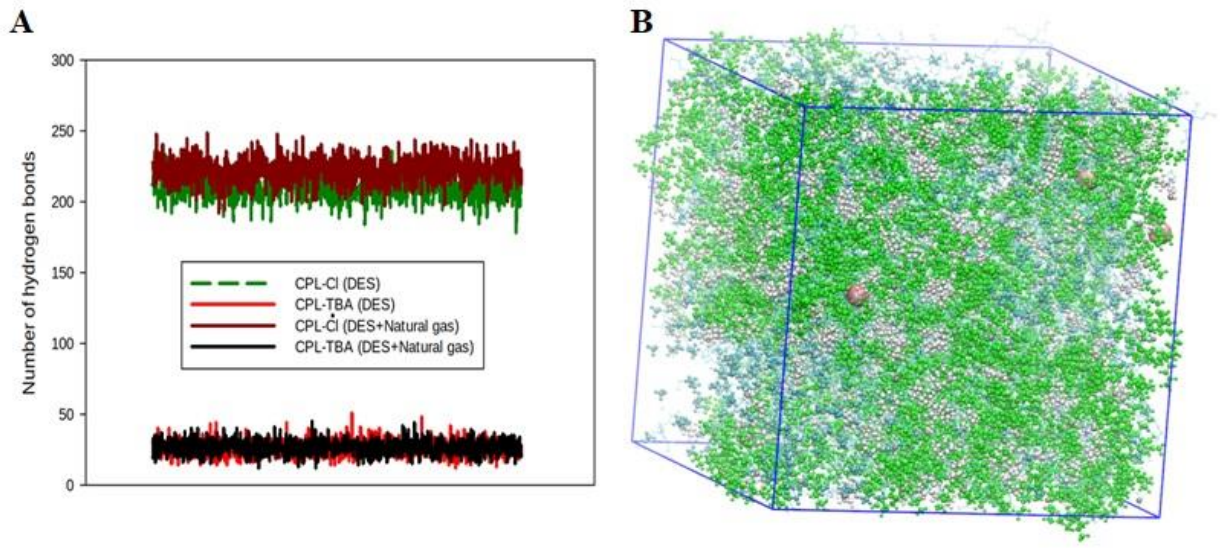

Figure 4.12: A) Hydrogen bonds between CPL-Cl, and CPL- TBA before and after mixing of DES with natural gas, B) Hydrogen sulfide molecules (reddish) surrounded by methane (blue) and DES (red & pink)

After investigating the DES formation, ab-initio and molecular dynamic simulations of the DES with hydrogen sulfides and methane's were performed to mimic the industrial natural gas sweetening process. Initially, DFT calculations were performed using B3LYP 6-311++G(d,p) level for geometry optimization of DES, H_2S, CH_4, and DES+H_2S+CH_4 in the gas phase. Next,

the most stable geometries of DES, H_2S, CH_4, and DES+H_2S+CH_4 in the gas phase were illustrated on Figure 4.13A. The results reveal that the hydrogen sulfide started to interact with chloride ion by hydrogen bonding (2.27 Å). Moreover, there were no interactions of methane with DES and H_2S as shown on Figure 4.13A. Interestingly, as shown in Figure 4.13B, the molecular electrostatic maps indicate that the negative charge (red) is localized between hydrogen sulfide and chloride ion due to delocolization of chlorine ion through hydrogen bonding with hydrogen sulfide.

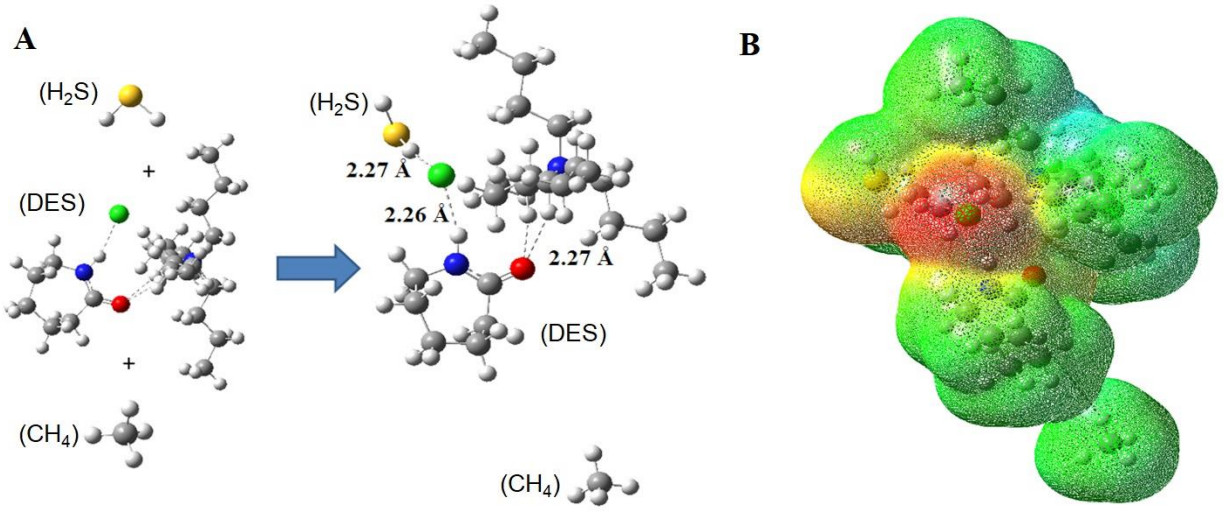

Figure 4.13: A) Optimized structures for H_2S, CH_4, DES, DES+H_2S+CH_4 and B) Molecular electrostatic maps for DES+H_2S+CH_4 systems in the gas phase

Moreover, *H-1*, *H*, *L*, *L+1* molecular orbital density illustration for DES+H_2S+CH_4 system is shown in Figure 4.14. In general, LUMO is formed around the TBACl and HOMO formed around the Cl ion and hydrogen sulfide. In addition, the higher molecular stability and lower chemical reactivity were observed for larger value of computed HOMO-LUMO gap (–4.99 eV).

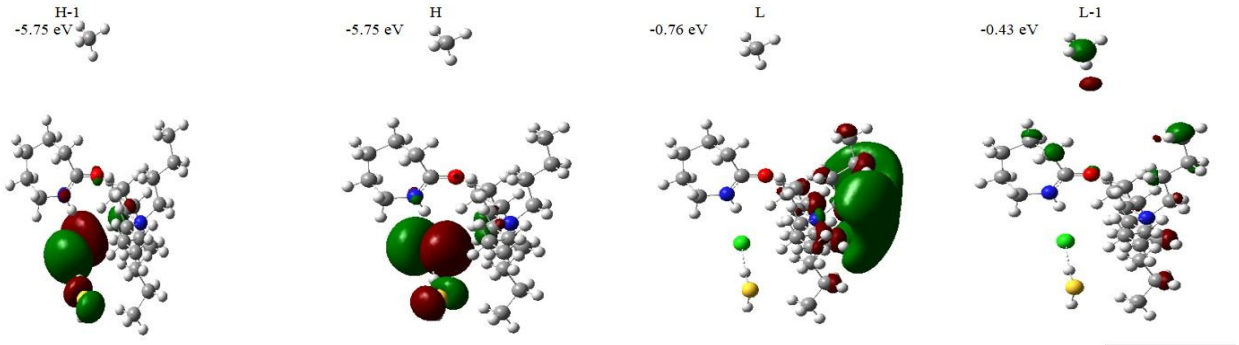

Figure 4.14: Representations (isovalue=0.02, isodensity=0.0004) of H-1, H, L, L+1 molecular

orbitals density for optimized electronic ground state geometries of DES + H_2S + CH_4.

4.3 Effect of process parameters on desulfurization

In this part concentration of hydrogen sulfide, effect of temperature and pressure on the process was investigated in detail.

4.3.1 Increasing hydrogen sulfide concentration

The next section of this thesis was performing molecular dynamics simulations to investigate how H_2S concentration affects the desulfurization process. Interestingly, in this work we performed molecular dynamics simulation with 5000/1000 ppm (system 7) concentrations of H_2S (high concentrations) to (i) conduct simulation within reasonable time, (ii) to study the effectiveness of these DES at high H_2S concentrations. The interaction energies of H_2S with methane, and DES were analyzed as shown on Figure 4.15. The results reveal that the increased of H_2S concentration before mixing contribute to rise of the interaction energy between H_2S and CH_4 from –0.99 kJ/mol (5000 ppm) to –4.98 kJ/mol (10000 ppm). Moreover, after mixing of H_2S and CH_4 with DES as shown on system 7, the desulfurization of natural gas at higher concentration of H_2S in CH_4 was evaluated. The results indicate that the interaction strength between H_2S and CH_4 were –0.12 kJ/mol (5000 ppm), –0.56 kJ/mol (10000 ppm) for system 7, while the interaction energies between H_2S and DES were –67.98 kJ/mol (5000 ppm), –124.66 kJ/mol (10000 ppm) for system 7. Basically, this means that after mixing H_2S and CH_4 with DES (CPL:TBACl), the H_2S/CH_4 interaction strength decreases which is leading to summary that the DES is able to absorb H_2S from the model natural gas. The results also imply that with an increasing H_2S concentration, the desulfurization efficiency comes down. Moreover, these DESs are highly effectively at low fuel (natural gas) ratio. For higher fuel and lower DES ratio, ~seven and three-fold increase in H_2S/CH_4 interaction energies were observed, which means lower extraction efficiency (Figure 15A and B).

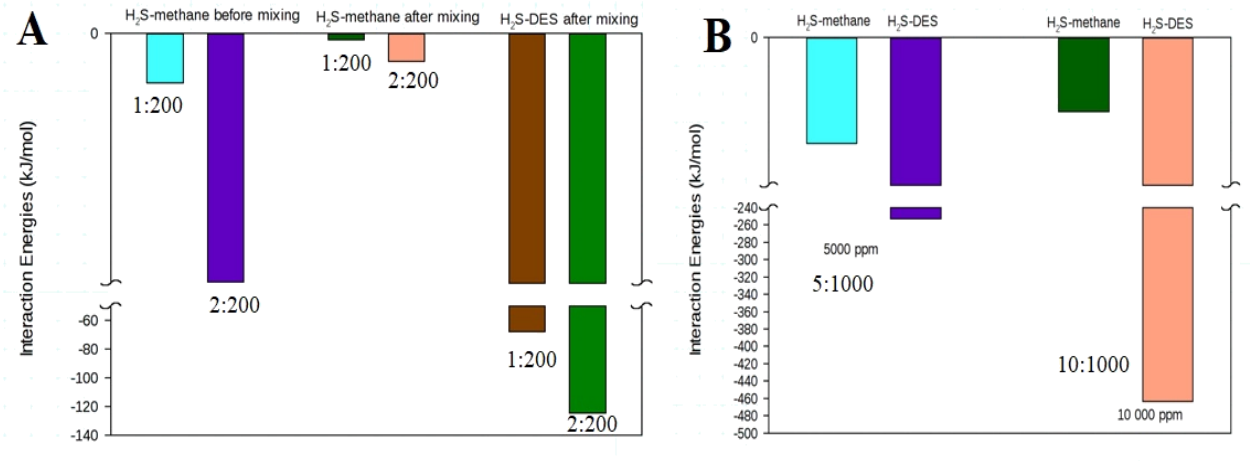

Figure 4.15: A) Interaction energies of H_2S/CH_4 before and after mixing, H_2S-DES after mixing, for systems B) Interaction energies of H_2S/CH_4 before and after mixing, H_2S-DES after mixing, for systems.

4.3.2 Increasing temperature and pressure

This part was completed successfully to explore how increase of T (K) and pressure (bar) could affect the desulfurization process. Consequently, the system 8 was selected for the simulation at 25^0C, 1 bar; 60^0C, 1 bar and 25^0C, 10 bar. The results imply that the desulfurization of natural gas was achieved, as the molecular interaction energies between H_2S and DES is higher than H_2S and CH_4 in all cases. For instance, H_2S-CH_4 interaction energies were –10.77 kJ/mol (25 ^{0}C), –15.31 kJ/mol (60 ^{0}C), and –12.87 kJ/mol, while H_2S-DES interaction energies are –252.84 kJ/mol (25 ^{0}C), –269.59 kJ/mol (60 ^{0}C) and –254.23 kJ/mol (10 bar). Moreover, there is insignificant difference for H_2S/CH_4 and H_2S/DES interaction energies between system simulated at different pressure and temperature, which proves that DES could be effective at the room temperature resulting in the less energy consumption during the natural gas sweetening process.

4.3.3 Comparison of various DESs on the absorption process

The Figure 4.16 illustrates the desulfurization of hydrogen sulfide from methane through four different DES; DES1 (CPL:TBABr), DES2 (CPL:TBACl), DES3 (ChCl:Urea), DES4 (MEA:MTPPBr). The results indicate that there is also insignificant difference for H_2S/DES

interaction energies between systems simulated. In addition, the results indicate that ChCl:Urea had strong H_2S/CH_4 interactions as compared to other DESs; however, the energy between H_2S and the DES were also strongest. MEA:MTPPBr, on the other hand, had ~two-fold increase in H_2S/CH_4 and had similar H_2S/DES as for CPL based DESs. In all the cases, H_2S was strongly interacting with the anion present in the DESs.

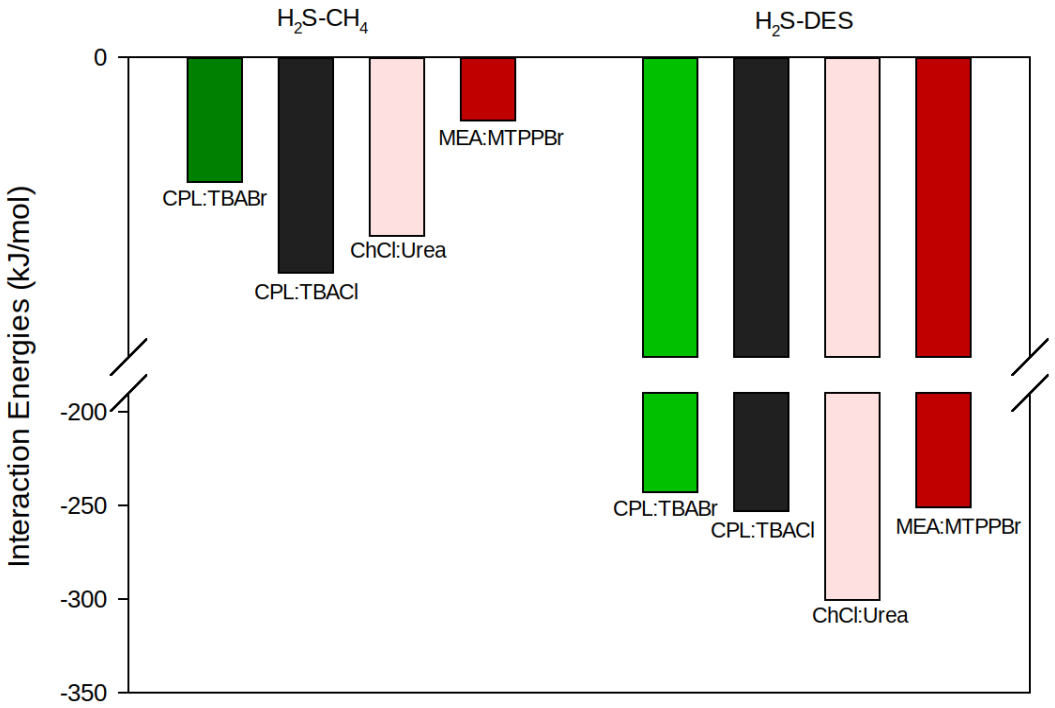

Figure 4.16: The interaction energies for various DESs

Chapter 5 – Conclusion and future work

Considering potential commercial applications of the CPL:TBABr, CPL:TBACl, as the DES were examined at molar ratio of 1:1, using molecular dynamics simulation and ab-initio calculation. The objective of this investigation was to understand intermolecular interactions within the formation of DES and also to study the desulfurization of natural gas by these DESs. Regarding the formation mechanism of the caprolactam DES, the results reveal weakening of interactions between CPL molecules. On the contrary, strong intermolecular interactions were observed between CPL/Br, and CPL/Cl respectively. We further observe a high number of hydrogen bonds between CPL/Br, and CPL/Cl. To explore desulfurization of natural gas, simulations were successfully performed on the mixtures of H_2S+CH_4+DES at different fuel to the DES mole ratio, at different temperatures and pressures. Furthermore, the absorption process of H_2S molecules by deep eutectic solvents (DESs) composed of CPL:TBABr (1:1), CPL:TBACl (1:1), ChCl:Urea (1:1), and MTPPBr:MEA (1:6) were studied using molecular dynamics and ab-initio simulation to understand the natural gas upgrading process, as the existing literature covers only experiments on the removal of pure hydrogen sulfide via the DESs. In particular, analyzed results indicate that H_2S/CH_4 interactions decreased significantly in the presence of DES. On the contrary H_2S/Br ion, and H_2S/Cl ion interactions strengthened. Comparing with different temperatures, pressures, we examined the absorption of H_2S by DES showed insignificant changes. Moreover, examination of ChCl:Urea (1:2), and MTPPBr:MEA (1:6), reveal that all these DES are capable of absorption H_2S, however; among all, CPL:TBACl is preferable.

Taken together, our proposed suggestion is that the experimental study on absorption of hydrogen sulfide by various DESs in the presence of methane is required. In addition, the process simulation of natural gas sweetening is required for these DESs via the implementation of Aspen Plus commercial chemical process simulator. The future works will be important to explore the

absorption of hydrogen sulfide and carbon dioxide simultaneously from natural gas using the DES. The results presented herein, lay a foundation to our understanding of the molecular interactions within the DESs and their interactions with hydrogen sulfide.

Reference

[1] W. A. Poe and S. Mokhatab, "Chapter 2 - Process Modeling and Simulation," W. A. Poe and S. B. T.-M. Mokhatab Control, and Optimization of Natural Gas Processing Plants, Eds. Boston: Gulf Professional Publishing, 2017, pp. 73–96.

[2] C.-A. Hwang, G. A. Iglesias-Silva, J. C. Holste, K. R. Hall, B. E. Gammon, and K. N. Marsh, "Densities of Carbon Dioxide + Methane Mixtures from 225 K to 350 K at Pressures up to 35 MPa," *J. Chem. Eng. Data*, vol. 42, no. 5, pp. 897–899, Sep. 1997, doi: 10.1021/je970042b.

[3] P. Roy and M. Amin, "Aspen-HYSYS simulation of natural gas processing plant," *J. Chem. Eng.*, vol. 26, pp.1-10, Mar. 2012, doi: 10.3329/jce.v26i1.10186.

[4] D. Shah, D. Gapeyenko, A. Urakpayev, and M. Torkmahalleh, "Molecular dynamics simulations on extractive desulfurization of fuels by tetrabutylammonium chloride based Deep Eutectic Solvents," *J. Mol. Liq.*, vol. 274, pp. 254–260, 2019, doi: 10.1016/j.molliq.2018.10.131.

[5] F.-Y. Liang, M. Ryvak, S. Sayeed, and N. Zhao, "The role of natural gas as a primary fuel in the near future, including comparisons of acquisition, transmission and waste handling costs of as with competitive alternatives," *Chem. Cent. J.*, vol. 6, pp. 1-10 Apr. 2012, doi: 10.1186/1752-153X-6-S1-S4.

[6] D. Shah and F. Mjalli, "Effect of Water on the Thermo-physical Properties of Reline: An Experimental and Molecular Simulation Based Approach," *Phys. Chem. Chem. Phys.*, vol. 16, pp.1-10, Aug. 2014, doi: 10.1039/C4CP02600D.

[7] T. Zhekenov, N. Toksanbayev, Z. Kazakbayeva, D. Shah, and F. Mjalli, "Formation of type III Deep Eutectic Solvents and effect of water on their intermolecular interactions," *Fluid Phase Equilib.*, vol. 1, pp. 1-10, Jan. 2017, doi: 10.1016/j.fluid.2017.01.022.

[8] D. Kussainova and D. Shah, "Monoethanolamine based DESs for CO_2 absorption: Insights from molecular dynamics simulations," *Sep. Purif. Technol.*, vol. 231, p. 115-125, 2020, doi: https://doi.org/10.1016/j.seppur.2019.115931.

[9] M. Espino, M. Fernández, F. Gomez, and M. Silva, "Natural designer solvents for greening analytical chemistry," *Trends Anal. Chem.*, vol. 76, pp. 126–136, Dec. 2015, doi: 10.1016/j.trac.2015.11.006.

[10] H. Ghanbarabadi and B. Khoshandam, “Simulation and comparison of Sulfinol solvent performance with Amine solvents in removing sulfur compounds and acid gases from natural sour gas,” *J. Nat. Gas Sci. Eng.*, vol. 22, pp. 415–420, 2015, doi: https://doi.org/10.1016/j.jngse.2014.12.024.

[11] K. Huang, X. Zhang, Y. Wu, and Y.-T. Wu, “Hydrophobic Protic Ionic Liquids Tethered with Tertiary Amine Group for Highly Efficient and Selective Absorption of H_2S from CO_2,” *AIChE J.*, vol. 62, pp. 1-10, Jun. 2016, doi: 10.1002/aic.15363.

[12] F.-Y. Jou, R. D. Deshmukh, F. D. Otto, and A. E. Mather, “Solubility of H_2S, CO_2 , CH_4 and C_2H_6 in sulfolane at elevated pressures,” *Fluid Phase Equilib.*, vol. 56, pp. 313–324, 1990, doi: https://doi.org/10.1016/0378-3812(90)85111-M.

[13] D. Kussainova and D. Shah, “Structure of monoethanolamine based type III DESs: Insights from molecular dynamics simulations,” *Fluid Phase Equilib.*, vol. 482, pp. 112–117, 2019, doi: https://doi.org/10.1016/j.fluid.2018.11.017.

[14] D. Shah, U. Mansurov, and F. Mjalli, “Intermolecular interactions and solvation effects of dimethylsulfoxide on type III deep eutectic solvents,” *Phys. Chem. Chem. Phys.*, vol. 21, pp.1-10, Jul. 2019, doi: 10.1039/C9CP02368B.

[15] P. Xu, G.-W. Zheng, M.-H. Zong, N. Li, and W.-Y. Lou, “Recent progress on deep eutectic solvents in biocatalysis.,” *Bioresour. Bioprocess.*, vol. 4, no. 1, p. 34, 2017, doi: 10.1186/s40643-017-0165-5.

[16] E. L. Smith, A. P. Abbott, and K. S. Ryder, “Deep Eutectic Solvents (DESs) and Their Applications,” *Chem. Rev.*, vol. 114, no. 21, pp. 11060–11082, Nov. 2014, doi: 10.1021/cr300162p.

[17] A. P. Abbott, D. Boothby, G. Capper, D. L. Davies, and R. K. Rasheed, “Deep Eutectic Solvents Formed between Choline Chloride and Carboxylic Acids: Versatile Alternatives to Ionic Liquids,” *J. Am. Chem. Soc.*, vol. 126, no. 29, pp. 9142–9147, Jul. 2004, doi: 10.1021/ja048266j.

[18] G. García, S. Aparicio, R. Ullah, and M. Atilhan, “Deep Eutectic Solvents: Physicochemical Properties and Gas Separation Applications,” *Energy & Fuels*, vol. 29, no. 4, pp. 2616–2644, Apr. 2015, doi: 10.1021/ef5028873.

[19] R. Stefanovic, M. Ludwig, G. B. Webber, R. Atkin, and A. J. Page, “Nanostructure, hydrogen bonding and rheology in choline chloride deep eutectic solvents as a function of the hydrogen bond donor,” *Phys. Chem. Chem. Phys.*, vol. 19, no. 4, pp. 3297–3306, 2017, doi: 10.1039/C6CP07932F.

[20] M. B. Taysun, E. Sert, and F. S. Atalay, “Effect of Hydrogen Bond Donor on the Physical Properties of Benzyltriethylammonium Chloride Based Deep Eutectic Solvents and Their Usage in 2-Ethyl-Hexyl Acetate Synthesis as a Catalyst,” *J. Chem. Eng. Data*, vol. 62, no. 4, pp. 1173–1181, Apr. 2017, doi: 10.1021/acs.jced.6b00486.

[21] F. S. Mjalli and D. Shah, “Simulation based insight into solvation properties of ferric chloride based eutectic solvent,” *Chem. Eng. Trans.*, vol. 43, pp. 1843–1848, 2015, doi: 10.3303/CET1543308.

[22] A. P. Abbott, J. C. Barron, K. S. Ryder, and D. Wilson, “Eutectic-based ionic liquids with metal-containing anions and cations.,” *Chemistry*, vol. 13, no. 22, pp. 6495–6501, 2007, doi: 10.1002/chem.200601738.

[23] R. Bernasconi, G. Panzeri, A. Accogli, F. Liberale, L. Nobili, and L. Magagnin, “Electrodeposition from Deep Eutectic Solvents,” Progress and Developments in Ionic Liquids, vol. 1, pp. 1-10, 2017.

[24] S. B. Phadtare and G. S. Shankarling, “Halogenation reactions in biodegradable solvent: Efficient bromination of substituted 1-aminoanthra-9,10-quinone in deep eutectic solvent (choline chloride : urea),” *Green Chem.*, vol. 12, no. 3, pp. 458–462, 2010, doi: 10.1039/B923589B.

[25] B. Singh, H. Lobo, and G. Shankarling, “Selective N-Alkylation of Aromatic Primary Amines Catalyzed by Bio-catalyst or Deep Eutectic Solvent,” *Catal. Letters*, vol. 141, pp. 178–182, Jan. 2011, doi: 10.1007/s10562-010-0479-9.

[26] R. Morales, V. Tambyrajah, P. Jenkins, D. Davies, and A. Abbott, “The regiospecific Fischer indole reaction in choline chloride·2$ZnCl_2$ with product isolation by direct sublimation from the ionic liquid,” *Chem. Commun. (Camb).*, vol. 2, pp. 158–159, Feb. 2004, doi: 10.1039/b313655h.

[27] S. Sarmad, J.-P. Mikkola, and X. Ji, “CO2 capture with Ionic liquids (ILs) and Deep Eutectic Solvents (DESs): a new generation of sorbents,” *ChemSusChem*, vol. 10, Dec. 2016, doi: 10.1002/cssc.201600987.

[28] N. Zulkurnai, U. Md Ali, N. Ibrahim, and N. Manan, “Carbon Dioxide (CO_2) Adsorption by Activated Carbon Functionalized with Deep Eutectic Solvent (DES),” *IOP Conf. Ser. Mater. Sci. Eng.*, vol. 206, p. 120-131, Jun. 2017, doi: 10.1088/1757-899X/206/1/012001.

[29] A. Zhu, T. Jiang, B. Han, J. Zhang, Y. Xie, and X. Ma, “Supported choline chloride/urea as a heterogeneous catalyst for chemical fixation of carbon dioxide to cyclic carbonates,” *Green Chem.*, vol. 9, no. 2, pp. 169–172, 2007, doi: 10.1039/B612164K.

[30] M. Francisco, A. van den Bruinhorst, L. F. Zubeir, C. J. Peters, and M. C. Kroon, “A new low transition temperature mixture (LTTM) formed by choline chloride+lactic acid: Characterization as solvent for CO_2 capture,” *Fluid Phase Equilib.*, vol. 340, pp. 77–84, 2013, doi: https://doi.org/10.1016/j.fluid.2012.12.001.

[31] C. Li *et al.*, “Extraction desulfurization process of fuels with ammonium-based deep eutectic solvents,” *Green Chem.*, vol. 15, no. 10, pp. 2793–2799, 2013, doi: 10.1039/C3GC41067F.

[32] C. Li *et al.*, “Extraction desulfurization of fuels with ‘metal ions’ based deep eutectic

solvents (MDESs)," *Green Chem.*, vol. 18, no. 13, pp. 3789–3795, 2016, doi: 10.1039/C6GC00366D.

[33] A. P. Abbott, P. M. Cullis, M. J. Gibson, R. C. Harris, and E. Raven, "Extraction of glycerol from biodiesel into a eutectic based ionic liquid," *Green Chem.*, vol. 9, no. 8, pp. 868–872, 2007, doi: 10.1039/B702833D.

[34] B. Guo, E. Duan, Y. Zhong, L. Gao, X. Zhang, and D. Zhao, "Absorption and Oxidation of H_2S in Caprolactam Tetrabutyl Ammonium Bromide Ionic Liquid," *Energy & Fuels*, vol. 25, no. 1, pp. 159–161, Jan. 2011, doi: 10.1021/ef1012006.

[35] F. Liu *et al.*, "Thermodynamic and Molecular Insights into the Absorption of H_2S, CO_2 and CH_4 in Choline Chloride plus Urea Mixtures," *AIChE J.*, vol. 1, pp. 1-10, Feb. 2019, doi: 10.1002/aic.16574.

[36] H. Wu, M. Shen, X. Chen, G. Yu, A. A. Abdeltawab, and S. M. Yakout, "New absorbents for hydrogen sulfide: Deep eutectic solvents of tetrabutylammonium bromide/carboxylic acids and choline chloride/carboxylic acids," *Sep. Purif. Technol.*, vol. 224, pp. 281–289, 2019, doi: https://doi.org/10.1016/j.seppur.2019.04.082.

[37] P. Podio-Guidugli, "On (Andersen–)Parrinello–Rahman Molecular Dynamics, the Related Metadynamics, and the Use of the Cauchy–Born Rule," *J. Elast.*, vol. 100, pp. 145–153, Jun. 2010, doi: 10.1007/s10659-010-9250-0.

[38] H. J. C. Berendsen, "Transport Properties Computed by Linear Response through Weak Coupling to a Bath," *Computer Simulation in Material Science*, vol 205, pp. 140-155, no. February, 2015, doi: 10.1007/978-94-011-3546-7.

[39] K. Koziara, M. Stroet, A. Malde, and A. Mark, "Testing and validation of the Automated Topology Builder (ATB) version 2.0: Prediction of hydration free enthalpies," *J. Comput. Aided. Mol. Des.*, vol. 28, Jan. 2014, doi: 10.1007/s10822-014-9713-7.

[40] G. García, M. Atilhan, and S. Aparicio, "Interfacial Properties of Deep Eutectic Solvents Regarding to CO_2 Capture," *J. Phys. Chem. C*, vol. 119, no. 37, pp. 21413–21425, Sep. 2015, doi: 10.1021/acs.jpcc.5b04585.

[41] F. Groenewald and J. Dillen, "Conformational analysis of caprolactam, cycloheptene and caprolactone," *Struct. Chem.*, vol. 23, pp. 723-735, Jun. 2012, doi: 10.1007/s11224-011-9921-x.

[42] W. Zaidi, A. Boisset, J. Jacquemin, L. Timperman, and M. Anouti, "Deep Eutectic Solvents Based on N-Methylacetamide and a Lithium Salt as Electrolytes at Elevated Temperature for Activated Carbon-Based Supercapacitors," *J. Phys. Chem. C*, vol. 118, no. 8, pp. 4033–4042, Feb. 2014, doi: 10.1021/jp412552v.

[43] S. Zhu *et al.*, "Vibrational analysis and formation mechanism of typical deep eutectic solvents: An experimental and theoretical study," *J. Mol. Graph. Model.*, vol. 68, pp. 158–175, 2016, doi: https://doi.org/10.1016/j.jmgm.2016.05.003.

[44] K. M. Manamela, L. Murulana, M. Kabanda, and E. Ebenso, “Adsorptive and DFT Studies of Some Imidazolium Based Ionic Liquids as Corrosion Inhibitors for Zinc in Acidic Medium,” *Int. J. Electrochem. Sci.*, vol. 9, pp. 3029–3046, Jun. 2014.

[45] E. B. Winn, “The Temperature Dependence of the Self-Diffusion Coefficients of Argon, Neon, Nitrogen, Oxygen, Carbon Dioxide, and Methane,” *Phys. Rev.*, vol. 80, no. 6, pp. 1024–1027, Dec. 1950, doi: 10.1103/PhysRev.80.1024.

[46] N. Sakoda and M. Uematsu, “A Thermodynamic Property Model for Fluid Phase Hydrogen Sulfide,” *Int. J. Thermophys. - INT J THERMOPHYS*, vol. 25, pp. 709–737, May 2004, doi: 10.1023/B:IJOT.0000034234.06341.8a.

[47] F. S. Mjalli, G. Murshid, S. Al-Zakwani, and A. Hayyan, “Monoethanolamine-based deep eutectic solvents, their synthesis and characterization,” *Fluid Phase Equilib.*, vol. 448, pp. 30–40, 2017, doi: https://doi.org/10.1016/j.fluid.2017.03.008.

[48] C. S. Pomelli, C. Chiappe, A. Vidis, G. Laurenczy, and P. J. Dyson, “Influence of the Interaction between Hydrogen Sulfide and Ionic Liquids on Solubility: Experimental and Theoretical Investigation,” *J. Phys. Chem. B*, vol. 111, no. 45, pp. 13014–13019, Nov. 2007, doi: 10.1021/jp076129d.

[49] F.-Y. Jou and A. Mather, “Solubility of Hydrogen Sulfide in [bmim][PF6],” *Int. J. Thermophys.*, vol. 28, pp. 490–495, Jun. 2007, doi: 10.1007/s10765-007-0185-z.

[50] A. H. Jalili, M. Rahmati-Rostami, C. Ghotbi, M. Hosseini-Jenab, and A. N. Ahmadi, “Solubility of H_2S in Ionic Liquids [bmim][PF_6], [bmim][BF_4], and [bmim][Tf_2N],” *J. Chem. Eng. Data*, vol. 54, no. 6, pp. 1844–1849, Jun. 2009, doi: 10.1021/je8009495.

[51] H. Sakhaeinia, A. H. Jalili, V. Taghikhani, and A. A. Safekordi, “Solubility of H_2S in Ionic Liquids 1-Ethyl-3-methylimidazolium Hexafluorophosphate ([emim][PF_6]) and 1-Ethyl-3-methylimidazolium Bis(trifluoromethyl)sulfonylimide ([emim][Tf_2N]),” *J. Chem. Eng. Data*, vol. 55, no. 12, pp. 5839–5845, Dec. 2010, doi: 10.1021/je100794k.

[52] K. Huang, X. Zhang, Y. Xu, Y. Wu, and X. Hu, “Protic Ionic Liquids for the Selective Absorption of H_2S from CO_2: Thermodynamic Analysis,” *AIChE J.*, vol. 60, pp.4232-4240, Dec. 2014, doi: 10.1002/aic.14634.

[53] K. Huang, D.-N. Cai, Y.-L. Chen, Y. Wu, X.-B. Hu, and Z.-B. Zhang, “Dual Lewis Base Functionalization of Ionic Liquids for Highly Efficient and Selective Capture of H_2S,” *Chempluschem*, vol. 79, pp. 241–249, Feb. 2014, doi: 10.1002/cplu.201300365.

[54] K. Huang, D. Cai, Y. Chen, Y. Wu, X. Hu, and Z. Zhang, “Thermodynamic validation of 1-alkyl-3-methylimidazolium carboxylates as task-specific ionic liquids for H_2S absorption,” *AIChE J.*, vol. 59, Jun. 2013, doi: 10.1002/aic.13976.

[55] M. B. Shiflett, A. M. S. Niehaus, and A. Yokozeki, “Separation of CO_2 and H_2S Using Room-Temperature Ionic Liquid [bmim][$MeSO_4$],” *J. Chem. Eng. Data*, vol. 55, no. 11, pp. 4785–4793, Nov. 2010, doi: 10.1021/je1004005.

[56] M. Shokouhi, M. Adibi, A. H. Jalili, M. Hosseini-Jenab, and A. Mehdizadeh, "Solubility and Diffusion of H_2S and CO_2 in the Ionic Liquid 1-(2-Hydroxyethyl)-3-methylimidazolium Tetrafluoroborate," *J. Chem. Eng. Data*, vol. 55, no. 4, pp. 1663–1668, Apr. 2010, doi: 10.1021/je900716q.

[57] A. H. Jalili, M. Safavi, C. Ghotbi, A. Mehdizadeh, M. Hosseini-Jenab, and V. Taghikhani, "Solubility of CO_2, H_2S, and Their Mixture in the Ionic Liquid 1-Octyl-3-methylimidazolium Bis(trifluoromethyl)sulfonylimide," *J. Phys. Chem. B*, vol. 116, no. 9, pp. 2758–2774, Mar. 2012, doi: 10.1021/jp2075572.

[58] A. H. Jalili, M. Shokouhi, G. Maurer, and M. Hosseini-Jenab, "Solubility of CO_2 and H_2S in the ionic liquid 1-ethyl-3-methylimidazolium tris(pentafluoroethyl)trifluorophosphate," *J. Chem. Thermodyn.*, vol. 67, pp. 55–62, 2013, doi: https://doi.org/10.1016/j.jct.2013.07.022.

[59] K. Huang, X.-M. Zhang, L.-S. Zhou, D.-J. Tao, and J.-P. Fan, "Highly efficient and selective absorption of H_2S in phenolic ionic liquids: A cooperative result of anionic strong basicity and cationic hydrogen-bond donation," *Chem. Eng. Sci.*, vol. 173, pp. 253–263, 2017, doi: https://doi.org/10.1016/j.ces.2017.07.048.

[60] Handy, Santoso, Widodo, Palgunadi, Soerawidjaja, and A. Indarto, "H_2S–CO_2 Separation Using Room Temperature Ionic Liquid [BMIM][Br]," *Sep. Sci. Technol.*, vol. 49, pp.1-10, Sep. 2014, doi: 10.1080/01496395.2014.908919.

[61] M. Nematpour, A. H. Jalili, C. Ghotbi, and D. Rashtchian, "Solubility of CO_2 and H_2S in the ionic liquid 1-ethyl-3-methylimidazolium trifluoromethanesulfonate," *J. Nat. Gas Sci. Eng.*, vol. 30, pp. 583–591, 2016, doi: https://doi.org/10.1016/j.jngse.2016.02.006.

Appendix A:

Table A.1: Solubility of H_2S in ILs and DESs

Solvents[a]	T/K	P/kPa	Solubility (mol H_2S/kg DES)	Ref.
[bmim][Cl]	298	1400	35.71	[48]
[bmim][BF_4]	298	1400	20.33	[48]
[bmim][PF_6]	298	1400	9.15	[48]
[bmim][PF_6]	298	1700	10.08	[49]
[bmim][TfO]	298	1400	13.33	[48]
[emmim][Tf_2N]	298	1400	11.33	[48]
[4mbnpy][Tf_2N]	298	1400	13.18	[48]
[bnpy] [Tf_2N]	298	1400	11.67	[48]
[bpy] [Tf_2N]	298	1400	19.45	[48]
[bmmim] [Tf_2N]	298	1400	8.75	[48]
[eetamine] [Tf_2N]	298	1400	7.15	[48]
[betamine] [Tf_2N]	298	1400	6.35	[48]
[mbpy] [Tf_2N]	298	1400	19.74	[48]
[emim] [Tf_2N]	298	1400	10.88	[48]
[bmim][BF_4]	303	124	0.48	[50]
[bmim][PF_6]	303	165	0.29	[50]
[bmim][Tf_2N]	303	94	0.18	[50]
[hmim][BF_4]	303	111	0.36	[36]
[hmim][PF_6]	303	138	0.23	[36]
[hmim][Tf_2N]	303	97	0.10	[36]
[emim][PF_6]	333	144	0.15	[51]

[emim][Tf_2N]	303	107	0.19	[51]
DMEAH[For]	303	100	1.13	[52]
DMEAH[AC]	303	100	1.85	[52]
MDEAH[For]	303	100	0.15	[52]
MDEAH[AC]	303	100	1.26	[52]
[N_{2224}][DMG]	333	100	3.35	[53]
[N_{2224}][IMA]	333	100	1.37	[53]
[emim][Lac]	303	100	2.03	[54]
[emim][Ace]	303	100	3.01	[54]
[emim][Pro]	303	100	3.17	[54]
[HOemim][PF_6]	303	133	0.14	[51]
[HOemim][Tf_2N]	303	156	0.28	[51]
[HOemim][TfO]	303	105	0.22	[51]
[emim][$EtSO_4$]	303	113	0.09	[55]
[bmim][$MeSO_4$]	298	100	0.65	[55]
[hemim][BF_4]	303	136	0.17	[56]
[C_8mim][Tf_2N]	303	93	0.19	[57]
[C_6mim][Tf_2N]	303	146	0.28	[57]
[C_8mim][PF_6]	303	128	0.029	[58]
[C_2mim][eFAP]	313	100	0.053	[57]
[P_{4444}][PhO]	313	100	2.52	[59]
[TMGH][PhO]	313	100	1.47	[59]
[hmim][PhO]	313	100	3.28	[59]
[DBUH][PhO]	313	100	3.19	[59]
[TMHDA][Tf_2N]	313	100	1.47	[11]
[BDMAEE][Tf_2N]	298	100	1.22	[11]
[TMPDA][Tf_2N]	298	100	0.40	[11]
BmimBr	298	100	0.15	[60]
C_2mim[Otf]	303	346	1.10	[61]
CPL/TBABr (1:1)	303	101	1.58	[34]

ChCl/Urea (1:1.5)	313	200	0.39	[35]
Pro/TBABr(1:1)	298	245	1.66	[36]
Ac/TBABr(1:1)	298	225	1.25	[36]
For/TBABr(1:1)	298	178	0.72	[36]
ChCl/Pro(1:2)	298	184	0.70	[36]
ChCl/Ac(1:2)	298	249	0.95	[36]
ChCl/For(1:2)	298	262	0.75	[36]

[a]Abbreviations of solvents were listed below:

[bmim][Cl] - 1-butyl-3-methylimidazolium chloride

[bmim][BF_4] - 1-butyl-3-methylimidazolium tetrafluoroborate

[bmim][BF_6] - 1-butyl-3-methylimidazolium hexafluorophosphate

[bmim][TfO] - 1-butyl-3-methylimidazolium trifluoromethanesulfonate

[emmim][Tf_2N] - 1-ethyl-2,3-dimethylimidazolium bis(trifluoromethyl sulfonyl)imide

[4mbnpy][Tf_2N] - N-butyl-4-methylpyridinium bis(trifluoromethylsulfonyl)imide

[bnpy] [Tf_2N] - (N-butylpiridinium bis(trifluoromethylsulfonyl)imide

[bmmim] [Tf_2N] - 2-methyl-N-methyl-N-butylimidazolium bis(trifluoromethylsulfonyl)imide

[eetamine] [Tf_2N] - N-ethyl-N,N-dimethyl-N-(2-hydroxyethyl)ammonium bis(trifluoromethylsulfonyl) imide

[betamine] [Tf_2N] - N-butyl-N,N-dimethyl-N-(2-hydroxyethyl) ammonium bis(trifluoro methylsulfonyl) imide

[mbpy] [Tf_2N] - N-benzyl-N-methylpyrrolidinium bis(trifluoromethylsulfonyl)imide

[emim] [Tf_2N] - (1-ethyl-3-methyl imidazolium bis(trifluoromethylsulfonyl)imide

[bmim][BF_4] - 1-butyl-3-methylimidazolium tetrafluoroborate

[bmim][PF_6] - 1-butyl-3-methylimidazolium hexafluorophosphate

[bmim][Tf_2N] - 1-butyl-3-methylimidazolium bis(trifluoromethylsulfonyl)imide

[hmim][BF_4] - 1-hexyl-3-methylimidazolium tetrafluoroborate

[hmim][PF_6] - 1-hexyl-3-methylimidazolium hexafluorophosphate

[hmim][Tf_2N] - 1-hexyl-3-methylimidazolium bis(trifluoromethylsulfonyl)imide

[emim][PF_6] - 1-ethyl-3-methylimidazolium hexafluorophosphate

[emim][Tf_2N] - 1-ethyl-3-methylimidazolium bis(trifluoromethylsulfonyl)imide

DMEAH[AC] - dimethylethanol ammonium acetate dimethylethanolammonium acetate

DMEAH[For] - dimethylethanol ammonium acetate dimethylethanolammonium formate

MDEAH[For] - methyldiethanolammonium formate

MDEAH[AC] - methyldiethanolammonium acetate

$[N_{2224}][DMG]$ - triethylbutylammonium N,N-dimethylglycinate

$[N_{2224}][IMA]$ - triethylbutylammonium imidazolylacetate

[emim][Lac] - 1-ethyl-3-methylimidazolium lactate

[emim][Ace] - 1-ethyl-3-methylimidazolium acetate

[emim][Pro] - 1-ethyl-3-methylimidazolium propionate

$[HOemim][PF_6]$ - 1-(2-hydroxyethyl)-3-methylimidazolium hexafluorophosphate

$[HOemim][Tf_2N]$ - 1-(2-hydroxyethyl)-3-methylimidazolium bis(trifluoromethyl sulfonyl)imide

[HOemim][TfO] - 1-(2-hydroxyethyl)-3-methylimidazolium trifluoromethanesulfonate

$[emim][EtSO_4]$ - 1-ethyl-3-methylimidazolium ethyl sulfate

$[bmim][MeSO_4]$ - 1-butyl-3-methylimidazolium methyl sulfate

$[hemim][BF_4]$ - 1-(2-hydroxyethyl)-3-methylimidazolium tetrafluoroborate

$[C_8mim][Tf_2N]$ - 1-octyl-3-methylimidazolium bis(trifluoromethyl)sulfonylimide

$[C_6mim][Tf_2N]$ - 1-hexyl-3-methylimidazolium bis(trifluoromethyl)sulfonylimide

$[C_8mim][PF_6]$ - 1-octyl-3-methylimidazolium hexafluorophosphate

$[C_2mim][eFAP]$ -1-ethyl-3-methylimidazolium tris(pentafluoroethyl)trifluorophosphate

$[P_{4444}][PhO]$ - tetraburylphosphonium phenolate

[TMGH][PhO] - tetramethylguanidinium phenolate

[hmim][PhO] - 1-hexyl-3-methylimidazolium phenolate

[DBUH][PhO] - 1,8-diazabicyclo[5.4.0]undec-7-ene-1-ium phenolate

$[TMHDA][Tf_2N]$ - N,N,N,N-tetramethyl-1,6-hexanediamine bis(trifluoromethylsulfonyl)imide

$[BDMAEE][Tf_2N]$ - bis(2-dimethylaminoethyl)ether bis(trifluoromethylsulfonyl)imide

$[TMPDA][Tf_2N]$ - N,N,N,N-tetramethyl-1,3-propanediamine bis(trifluoromethylsulfonyl)imide

BmimBr - 1-butyl-3-methylimidazolium bromide

$C_2mim[Otf]$ - 1-ethyl-3-methylimidazolium trifluoromethanesulfonate